The Astrophysical Journal, 698:895–910, 2009 June 10 doi:10.1088/0004-637X/698/1/895

ARE THE VARIATIONS IN QUASAR OPTICAL FLUX DRIVEN BY THERMAL FLUCTUATIONS?

Brandon C. Kelly[1,2,3], Jill Bechtold[2], and Aneta Siemiginowska[1]
[1] Harvard-Smithsonian Center for Astrophysics, 60 Garden Street, Cambridge, MA 02138, USA; bckelly@cfa.harvard.edu
[2] Department of Astronomy, University of Arizona, Tucson, AZ 85721, USA
Received 2008 November 16; accepted 2009 April 3; published 2009 May 26

ABSTRACT

We analyze a sample of optical light curves for 100 quasars, 70 of which have black hole mass estimates. Our sample is the largest and broadest used yet for modeling quasar variability. The sources in our sample have $z < 2.8$, $10^{42} \lesssim \lambda L_\lambda(5100\ \text{Å}) \lesssim 10^{46}$, and $10^6 \lesssim M_{\rm BH}/M_\odot \lesssim 10^{10}$. We model the light curves as a continuous time stochastic process, providing a natural means of estimating the characteristic timescale and amplitude of quasar variations. We employ a Bayesian approach to estimate the characteristic timescale and amplitude of flux variations; our approach is not affected by biases introduced from discrete sampling effects. We find that the characteristic timescales strongly correlate with black hole mass and luminosity, and are consistent with disk orbital or thermal timescales. In addition, the amplitude of short-timescale variations is significantly anticorrelated with black hole mass and luminosity. We interpret the optical flux fluctuations as resulting from thermal fluctuations that are driven by an underlying stochastic process, such as a turbulent magnetic field. In addition, the intranight variations in optical flux implied by our empirical model are $\lesssim$0.02 mag, consistent with current microvariability observations of radio-quiet quasars. Our stochastic model is therefore able to unify both long- and short-timescale optical variations in radio-quiet quasars as resulting from the same underlying process, while radio-loud quasars have an additional variability component that operates on timescales $\lesssim$1 day.

Key words: accretion, accretion disks – galaxies: active – methods: data analysis – quasars: general

Online-only material: machine-readable tables

1. INTRODUCTION

It is widely accepted that the extraordinary activity associated with quasars[4] involves accretion onto a supermassive black hole, with the ultraviolet (UV)/optical emission arising from a geometrically thin, optically thick cold accretion disk. Aperiodic variability across all wavebands is ubiquitous in the AGN, with the most rapid variations occurring in the X-rays (for a review, see Ulrich et al. 1997). The source of quasar variability is unclear, and several models have been proposed for describing the optical variability of quasars, including accretion disk instabilities (e.g., Kawaguchi et al. 1998), supernovae (e.g., Aretxaga et al. 1997), microlensing (Hawkins 2000), and more general Poisson process models (e.g., Cid Fernandes et al. 2000). However, recent results from reverberation mapping have shown that the broad emission lines respond to variations in the continuum emission after some time lag (e.g., Peterson et al. 2004), implying that the continuum variations are dominated by processes intrinsic to the accretion disk. If the optical/UV variations are intrinsic to the accretion disk, then thermal fluctuations appear to be a natural choice for driving the optical/UV variations, as the optical/UV emission is thought to be thermal emission from the accretion disk. The fact that quasars become bluer as they brighten is consistent with a thermal origin (e.g., Giveon et al. 1999; Trèvese et al. 2001; Geha et al. 2003). Moreover, the thermal timescale is sensitive to the disk viscosity. Variability is therefore a potentially important and powerful probe of the quasar central engine and accretion disk physics.

A considerable amount of our interpretation and understanding of AGN accretion disks, and consequently their optical/UV emission, is based on the so-called α prescription (Shakura & Syunyaev 1973). Within the standard α model, the viscosity, thought to be the source of the thermal disk emission and outward transfer of angular momentum, is parameterized as being proportional to the total pressure in the disk. Previous work on estimating α from quasar variability has found a value of $\alpha \sim 0.01$ (e.g., Siemiginowska & Czerny 1989; Collier & Peterson 2001; Starling et al. 2004). However, when the disk is dominated by radiation pressure, as is thought to be the case in the inner regions, an α-disk is both thermally and viscously unstable (Shakura & Syunyaev 1976; Lightman & Eardley 1974). In particular, for a radiation-pressure-dominated disk, the thermal instability is expected to grow exponentially on a timescale similar to the thermal timescale. For AGN, the thermal timescale is on the order of months to years, and in general there is no evidence for instabilities in the optical light curves of AGNs which span $\gtrsim t_{\rm th}$ (e.g., Collier & Peterson 2001). However, the optical light curves for a few sources may show evidence of instability on a thermal timescale (e.g., Czerny et al. 2003; Lub & de Ruiter 1992).

If the stress is not proportional to the total pressure, but rather some other combination of the gas and radiation pressure, then the disk becomes more stable to thermal perturbations (e.g., Stella & Rosner 1984; Szuszkiewicz 1990; Merloni & Fabian 2002; Merloni 2003). Alternatively, if part of the accretion energy is dissipated in a hot corona, then there is no longer any runaway heating in the disk, as additional cooling is provided by the corona (Svensson & Zdziarski 1994). For example, disk models with alternative prescriptions for α, as well as the addition of a corona and jet, have been able to reproduce the variability of the microquasar GRS 1915+105 (Nayakshin et al. 2000; Janiuk et al. 2000, 2002). Previous work on three-dimensional magnetohydrodynamic (MHD) simulations of radiation-pressure-dominated AGN accretion disks have not

[3] Hubble Fellow.
[4] Throughout this work we will use the terms quasar and active galactic nucleus (AGN) to refer generically to broad-line AGNs. No luminosity difference between the two is assumed.

observed a thermal instability (e.g., Turner 2004; Hirose et al. 2008). Moreover, the most promising physical mechanism behind the viscous torque is the magnetorotational instability (MRI; Balbus & Hawley 1991, 1998), and recent numerical and analytical work has suggested that the α prescription may be a poor representation for MRI-driven viscosity (Pessah et al. 2008). Variability studies can therefore lend observational insight into the inadequacies of the traditional α prescription, and possibly lead to a more accurate characterization of the relationship between stress and pressure in the accretion disk.

A successful model for quasar X-ray variability describes the X-ray variations on long timescales as being the result of perturbations in the accretion rate that occur outside of the X-ray emitting region (e.g., Lyubarskii 1997; Mayer & Pringle 2006; Janiuk & Czerny 2007). These accretion rate perturbations then travel inward, modulating the X-ray emitting region. It has been suggested that the origin of such perturbations is the result of a magnetic field randomly varying in time, and may be related to the appearance of an outflow (King et al. 2004). If this model for the X-ray variability is correct, we would expect to also see variations in the optical luminosity, whose origin lies in the disk at radii farther from the central source. Therefore, understanding the origin of quasar optical variations will not only lead to a better understanding of accretion disk physics, but may also lead to a better understanding of the origin of quasar X-ray variability, possibly unifying the source of variability in the two bands.

Quasars have also been observed to vary on timescales as short as hours (so-called "microvariability" or "intranight variability"; Gopal-Krishna et al. 2003; Stalin et al. 2004, 2005; Gupta & Joshi 2005; Carini et al. 2007). Microvariability is known to be stronger in radio-loud quasars, especially blazars (e.g., Gupta & Joshi 2005), while microvariability in radio-quiet quasars is usually not detected above the photometric uncertainty (e.g., Gupta & Joshi 2005; Carini et al. 2007). The enhanced level of microvariability in radio-loud objects suggests that it is due to processes in a jet, while the physical cause of microvariability in radio-quiet objects has remained a puzzle. Reprocessing of X-rays, disk instabilities, or a weak blazar component have been suggested (Czerny et al. 2008).

There have been numerous previous investigations of quasar optical variability. However, because of the difficulty in obtaining high-quality, well-sampled light curves that cover a long time span, most previous work has involved ensemble studies of quasars, or analysis of simple correlations involving variability amplitude. The most well-known result from previous work is a tendency for AGNs to become less variable as their luminosity increases (e.g., Hook et al. 1994; Garcia et al. 1999; Giveon et al. 1999; Geha et al. 2003; Vanden Berk et al. 2004; de Vries et al. 2005, and references therein). There have also been claims of a variability–redshift correlation (e.g., Cristiani et al. 1990; Cid Fernandes et al. 1996; Cristiani et al. 1996; Trèvese & Vagnetti 2002), although the sign of this correlation varies between studies (e.g., see the list in Giveon et al. 1999). If real, the variability–redshift correlation is most likely caused by the fact that quasars are more variable at shorter wavelengths (e.g., Cutri et al. 1985; di Clemente et al. 1996; Helfand et al. 2001; Vanden Berk et al. 2004), corresponding to regions in the disk closer to the central black hole. Recently, a correlation between optical variability and black hole mass has been claimed (Wold et al. 2007). While many of these correlations are formally statistically significant, they often exhibit considerable scatter when one measures variability for individual objects.

A few previous studies have employed spectral techniques, such as power spectra and structure functions, in the analysis of quasar optical light curves. From these studies it has been inferred that quasar optical light curves generally have variations of $\sim$10% on timescales of months, and that the power spectra of optical light curves is well described as $P(f) \propto 1/f^2$ (Giveon et al. 1999; Collier & Peterson 2001; Czerny et al. 2003); power spectra of this form are consistent with random walk, or more generally, autoregressive processes. In addition, Collier & Peterson (2001) analyzed a sample of optical light curves from eight low-z Seyfert 1 galaxies. They found that the characteristic timescales of optical variations for the AGN in their sample are $\sim$10–100 days and correlate with black hole mass, consistent with disk orbital or thermal timescales. Czerny et al. (1999) found evidence for a flattening of the optical power spectrum of NGC 5548 on timescales longer than $\sim$100 days. Both Czerny et al. (1999, 2003) also suggested that the long-timescale optical variability was due to thermal fluctuations in the accretion disks of NGC 5548 and NGC 4151, respectively.

Motivated by the potential in variability studies for increasing our understanding of the structure of quasar accretion disks, we have compiled a sample of well sampled optical light curves from the literature. We directly model the quasar optical light curves as a stochastic process, in contrast to previous work based on more traditional Fourier (i.e., spectral) techniques. Our method allows us to describe quasar light curves with three free parameters: a characteristic timescale, amplitude of short-timescale variability, and the mean value of the light curve. In addition, our method enables us to estimate the characteristic timescale of quasar variations without the windowing effects that can bias spectral approaches. Our sample consists of 100 AGN, 70 of which have black hole mass estimates. The sources in our sample have $z < 2.8$, $10^{42} \lesssim \lambda L_\lambda(5100\ \text{Å}) \lesssim 10^{46}$, and $10^6 \lesssim M_{\rm BH}/M_\odot \lesssim 10^{10}$, making this by far the largest sample yet used for this kind of study.

In this work, we adopt a cosmology based on the *Wilkinson Microwave Anisotropy Probe* results ($h = 0.71, \Omega_m = 0.27, \Omega_\Lambda = 0.73$; Spergel et al. 2003).

2. DATA

In this work, we analyze a sample of 100 quasar optical light curves, compiled from the literature. Our sample consists of 55 AGNs from the *MACHO* survey (Geha et al. 2003), 37 Palomar Green (PG) quasars from the sample of Giveon et al. (1999), and eight Seyfert galaxies from the AGN Watch[5] database. We were able to obtain black hole mass estimates for 71 of the AGNs, where $M_{\rm BH}$ has been estimated for 20 of them from reverberation mapping (Peterson et al. 2004), and $M_{\rm BH}$ is estimated for the remaining 51 AGNs from the broad emission lines using standard scaling relationships (e.g., Vestergaard & Peterson 2006). Our sample is summarized in Table 1.

2.1. MACHO Quasars from Geha et al. (2003)

We collected R-band light curves from AGNs selected by the *MACHO* survey based on their variability (Alcock et al. 1997, 1999). The motivation for the *MACHO* survey was to study Galactic microlensing events behind the Magellanic Clouds. However, the survey was also able to select quasars via their variability, confirmed via spectroscopic follow-up, producing 59 quasars with well sampled light curves over a broad range

[5] http://www.astronomy.ohio-state.edu/agnwatch/

Table 1
Quasars Analyzed in this Work

R.A. (J2000)	Decl. (J2000)	z	$\log \lambda L_\lambda$(5100 Å) (erg s^{-1})	$\log M_{\rm BH}$ ($M_\odot$)	Err. in $\log M_{\rm BH}$[a]	Ref.[b]
00 29 13.7	+13 16 03.9	0.142	45.02	8.59	0.10	1
00 47 15.8	−72 41 12.2	0.530	44.34	···	···	2
00 49 34.4	−72 13 09.0	0.610	44.56	···	···	2
00 51 16.9	−72 16 51.1	0.330	44.00	···	···	2
00 54 52.1	+25 25 39.0	0.155	44.96	8.56	0.08	1
00 55 34.2	−72 28 30.0	1.660	45.69	···	···	2
00 55 59.6	−72 52 45.1	0.170	43.74	···	···	2
01 01 27.8	−72 46 14.4	1.720	45.52	···	···	2
01 02 14.4	−73 16 26.8	1.640	45.47	···	···	2
01 02 34.7	−72 54 22.2	0.220	43.93	···	···	2
01 07 21.7	−72 48 45.8	0.280	44.14	···	···	2
04 46 11.0	−72 05 09.0	0.900	45.08	···	···	2
04 53 56.6	−69 40 36.0	0.460	45.19	8.41	0.45	2
04 56 14.2	−67 39 10.8	2.220	45.22	···	···	2
05 00 17.6	−69 32 16.3	1.050	44.93	···	···	2

Notes.
[a] 1σ uncertainty on $\log M_{\rm BH}$.
[b] Reference for the optical light curve data.
References. (1) Giveon et al. (1999); (2) Geha et al. (2003); (3) Stirpe et al. (1994); (4) Peterson et al. (2000); (5) Kaspi et al. (1996); (6) Santos-Lleó et al. (2001); (7) Peterson et al. (2002); (8) Carone et al. (1996); (9) Shemmer et al. (2001); (10) Collier et al. (1998).
(This table is available in its entirety in a machine-readable form in the online journal. A portion is shown here for guidance regarding its form and content.)

in redshift ($0.1 \lesssim z \lesssim 2.8$; Geha et al. 2003). The quasar light curves span ∼7.5 yr, and have a typical sampling interval of ∼2–10 days, although much longer gaps exist for some light curves. In general, the *MACHO* light curves are the highest quality in our sample, often being frequently and regularly sampled. However, we note that because the *MACHO* sources were selected based on their variability, this sample is biased toward more variable objects. See Geha et al. (2003) for more details of the *MACHO* quasar catalog.

Spectra for the *MACHO* quasars are presented in Geha et al. (2003), and spectra for 27 of these quasars were kindly provided to us by Marla Geha. We calculated black hole mass estimates from the source luminosity and the FWHM of the Hβ, Mg II, or C IV broad emission line using standard scaling relationships (e.g., Vestergaard & Peterson 2006; Vestergaard & Osmer 2009). However, the spectra are not flux-calibrated, so the luminosities at 1350, 3000, and 5100 Å were estimated from the photometric data, assuming a power-law continuum with $\alpha = 0.5$, $f_\nu \propto \nu^{-\alpha}$ (Richards et al. 2001). Typical uncertainties on the broad-line mass estimates are ∼0.4 dex (e.g., Vestergaard & Peterson 2006). When combined with the measurement error in the FWHM measurements, and the uncertainty due to the intrinsic scatter in quasar spectral slopes (∼0.3; Richards et al. 2001), our typical adopted uncertainty in $M_{\rm BH}$ was ∼0.45 dex for the *MACHO* quasars.

2.2. PG Quasars from Giveon et al. (1999)

Giveon et al. (1999) report *B* and *R* photometric light curves for 42 PG quasars spanning ∼7 yr with a typical sampling interval of ∼40 days. These quasars are all bright ($B < 16$ mag) and nearby ($z < 0.4$). Peterson et al. (2004) report estimates of $M_{\rm BH}$ and L_λ(5100 Å) calculated from reverberation mapping for 12 of these quasars. Estimates of $M_{\rm BH}$ and L_λ(5100 Å) were taken from Vestergaard & Peterson (2006) for the remaining Giveon et al. (1999) quasars. See Giveon et al. (1999) for further details.

2.3. Seyfert Galaxies from AGN Watch Database

The light curves for the remaining eight AGNs in our sample are from the AGN Watch project. The optical light curves for the Seyfert Galaxies AKN 564, Fairall 9, MRK 279, MRK 509, NGC 3783, NGC 4051, NGC 4151, NGC 5548, and NGC 7469 were taken from the AGN Watch Web site. In general, we used the light curves at 5100 Å, with the exception of AKN 564, for which we used the *R*-band light curve. We excluded 3C390.3 from our analysis because it is a classified as an optically violent variable, and thus may experience a different variability mechanism than the other AGNs in our sample. Black hole masses and 5100 Å luminosities were taken from Peterson et al. (2004). Further details may be found in the references listed in Table 1. Although the AGN Watch sample is small compared to the other two, these sources are particularly important in our analysis because they help to anchor the low-*L* and low-$M_{\rm BH}$ end of the correlations analyzed in Section 4.

3. THE STATISTICAL MODEL: CONTINUOUS AUTOREGRESSIVE PROCESS

The previous analysis of Giveon et al. (1999) and Collier & Peterson (2001) suggests that the optical variability can be well described by a power-law power spectrum with slope ∼2. The power spectra of the *MACHO* quasars have not been analyzed for individual objects, although Hawkins (2007) investigated the power spectra of the ensemble of objects. In Figure 1, we show the geometric mean *R*-band power spectra for the *MACHO* quasars, along with the 90% confidence region on the geometric mean. The power spectra for the *MACHO* sources are well described by a power law of slope ∼2, consistent with previous work. The lack of any peaks in the power spectra, as well as the aperiodic and noisy appearance of quasar light curves, suggests that quasar light curves are stochastic or chaotic in nature.

In this work, we model quasar light curves as a *continuous time first-order autoregressive process* (CAR(1)). Power spectra

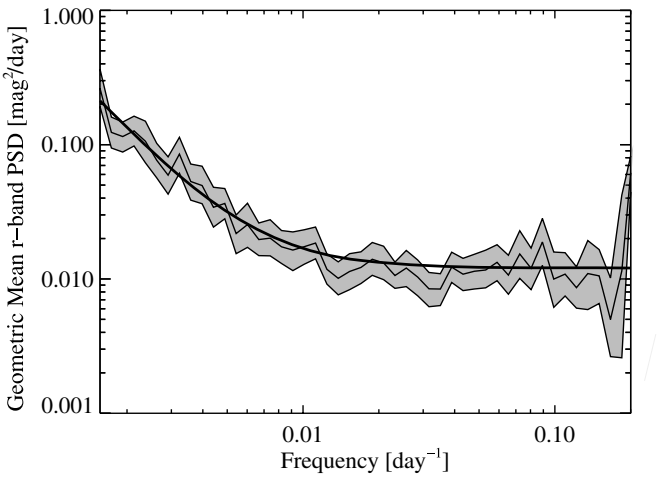

Figure 1. Geometric mean power spectrum (solid noisy line) for the *R*-band light curves of the *MACHO* quasars, along with 90% confidence region (shaded region). The thick solid line is a power spectrum of the form $P(f) \propto 1/f^2$ with an additive measurement error contribution. The optical light curves for the *MACHO* quasars are well described by a $1/f^2$ power spectrum, consistent with other samples of quasars. Power spectra of the form $1/f^2$ are suggestive of random walk and related stochastic processes.

of the form $P(f) \propto 1/f^2$ are consistent with a first-order autoregressive (AR(1)) process. We model this stochastic process in continuous time, both because the actual physical processes in the accretion disk are continuous, and because doing so allows a natural way of handling the irregular sampling of our light curves. Moreover, this process is well studied, only has three parameters, and provides a natural and consistent way of estimating a characteristic timescale and variance of quasar light curves.

The CAR(1) process is described by the following stochastic differential equation[6] (e.g., Brockwell & Davis 2002):

$$dX(t) = -\frac{1}{\tau}X(t)dt + \sigma\sqrt{dt}\epsilon(t) + b\,dt, \quad \tau, \sigma, t > 0. \quad (1)$$

Here, τ is called the "relaxation time" of the process $X(t)$, and $\epsilon(t)$ is a white noise process with zero mean and variance equal to 1. Within the context of this work, $X(t)$ is the quasar flux. We assume that the white noise process is also Gaussian. The mean value of $X(t)$ is $b\tau$ and the variance is $\tau\sigma^2/2$. Further details on the CAR(1) process are described in the Appendix.

The relaxation time, τ, can be interpreted as the time required for the time series to become roughly uncorrelated, and σ can be interpreted as describing the variability of the time series on timescales short compared to τ. Within the context of this work, $X(t)$ is the quasar light curve. It is tempting to associate τ with a characteristic timescale, such as the time required for diffusion to smooth out local accretion rate perturbations, and σ to represent the variability resulting from local random deviations in the accretion disk structure, such as caused by turbulence and other random MHD effects.

The power spectrum of a CAR(1) process is

$$P_X(f) = \frac{2\sigma^2\tau^2}{1 + (2\pi\tau f)^2}. \quad (2)$$

[6] Strictly speaking, the stochastic differential equation is complicated by the fact that white noise does not exist as a derivative in the usual sense. However, we ignore the mathematical technicalities for ease of interpretation of Equation (1).

From Equation (2), we infer that there are two important regimes for $P_X(f)$: $P_X(f) \propto 1/f^2$ for $f \gtrsim (2\pi\tau)^{-1}$ and $P_X(f) \propto$ constant for $f \lesssim (2\pi\tau)^{-1}$. Therefore, the CAR(1) process has a power spectrum that falls off as $1/f^2$ at timescales short compared to the relaxation time, and flattens to white noise at timescales long compared to the relaxation time. Because "characteristic" timescales of quasar light curves are often defined by a break in the power spectrum, this is an additional justification of associating τ with a characteristic timescale. In addition, because the power spectra of quasar optical light curves are well described by $P_X(f) \propto 1/f^2$, it suggests that a CAR(1) process should provide a good description of the light curves, with τ being on the order of the length of the light curves or longer.

To illustrate the CAR(1) process, we simulate four CAR(1) light curves. The light curves were simulated by first simulating a random variable from a normal distribution with mean τb and variance $\tau\sigma^2/2$; note that this is the mean and variance of the CAR(1) process. Then, from this random initial value, we simulated the rest of the light curve using Equations (A4) and (A5) in the Appendix. These simulated light curves span a length of 7 yr and are sampled every 5 days. The simulated light curves span a period in time similar to the quasar light curves analyzed in this work, but are better sampled than most of the quasar light curves. Three characteristic timescales of interest for quasars are the light crossing time, the gas orbital timescale, and the accretion disk thermal timescale. These timescales are

$$t_{\rm lc} = 1.1 \times \left(\frac{M_{\rm BH}}{10^8\,M_\odot}\right)\left(\frac{R}{100R_S}\right) \text{ days}, \quad (3)$$

$$t_{\rm orb} = 104 \times \left(\frac{M_{\rm BH}}{10^8\,M_\odot}\right)\left(\frac{R}{100R_S}\right)^{3/2} \text{ days}, \quad (4)$$

$$t_{\rm th} = 4.6 \times \left(\frac{\alpha}{0.01}\right)^{-1}\left(\frac{M_{\rm BH}}{10^8\,M_\odot}\right)\left(\frac{R}{100R_S}\right)^{3/2} \text{ yr}, \quad (5)$$

where $M_{\rm BH}$ is the mass of the black hole, R is the emission distance from the central black hole, $R_S = 2GM_{\rm BH}/c^2$ is the Schwarzschild radius, and α is the standard disk viscosity parameter. For the simulated quasar light curves, we use $M_{\rm BH} = 10^8\,M_\odot$, $\alpha = 0.01$, and $R = 100R_S$, and set τ equal to each of these three timescales. In addition, we use $b = 0$ and $\sigma = 1$. Note that the assumed value of α only affects the thermal timescale, and a higher value of α results in a shorter timescale.

The simulated light curves are shown in Figure 2, and their corresponding power spectra are shown in Figure 3. The increased amount of variation on long timescales with increasing τ is apparent. In addition, because $t_{\rm lc}$ is shorter than the time sampling, the first simulated light curve is only sampling frequencies on the flat part of the power spectrum, giving it the appearance of white noise. In contrast, the two simulated light curves with the longest timescales are sampled on the $1/f^2$ part of the power spectrum, giving them more of a "red noise" appearance. In addition, "red noise" leak affects the estimated power spectrum of the light curve with $\tau = 4.6$ yr, evidenced by the constant offset between the true power spectrum and the estimated one. Red noise leak occurs when power from timescales longer than the span of the time series "leaks" into the shorter timescales, biasing the power spectrum when estimated as the modulus of the discrete Fourier transform (e.g., van der Klis 1997).

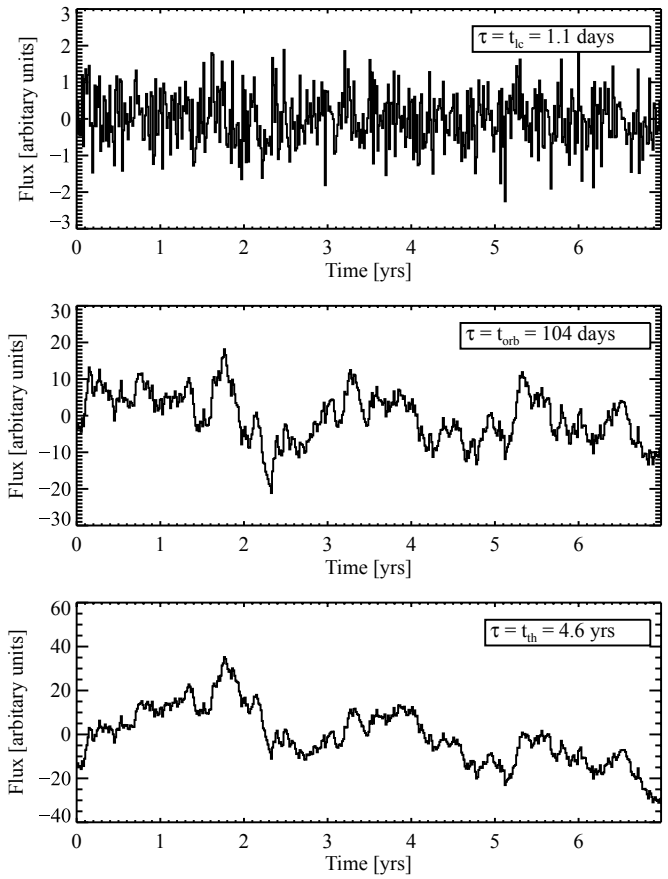

Figure 2. Light curves simulated from a CAR(1) process for three different characteristic timescales, assuming typical parameters for quasars ($M_{\rm BH} = 10^8\ M_\odot, R_s = 100, \alpha = 0.01$; see Equation (3)–(5)). From top to bottom, these are the light crossing time, $\tau = 1.1$ days, the disk orbital timescale, $\tau = 104$ days, and the disk thermal timescale, $\tau = 4.6$ yr. The stochastic nature of the CAR(1) process is apparent, and the light curve exhibits more variability on longer timescales as the characteristic timescale increases.

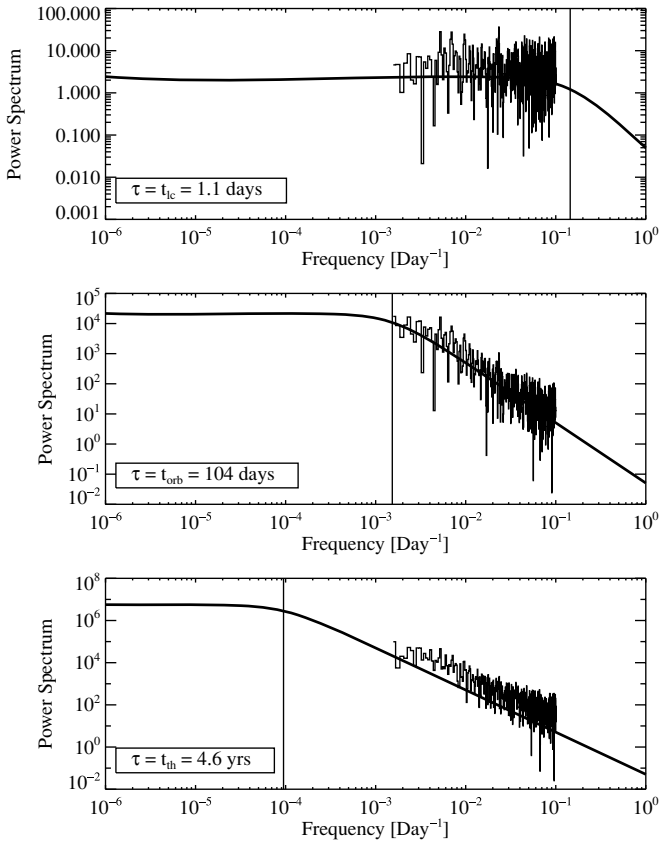

Figure 3. Power spectra for the simulated CAR(1) light curves shown in Figure 2. The actual power spectra are shown with a solid line, and the empirical power spectra estimated directly from the light curves are the noisy curves. The power spectra are flat on the "white noise" part of the curve, corresponding to frequencies $f \lesssim (2\pi\tau)^{-1}$, and fall off as $1/f^2$ on the "red noise" part of the curve, $f \gtrsim (2\pi\tau)^{-1}$. As τ increases, the break in the power spectra, marked with a vertical line, shifts toward smaller frequencies. For the CAR(1) process with $\tau = t_{\rm th}$, red noise leak biases the power spectrum estimated directly from the simulated light curve.

3.1. Estimating the Parameters of a CAR(1) Process

The parameters for a CAR(1) process are commonly estimated by maximum likelihood directly from the observed time series. This is an advantage over nonparametric approaches, such as the discrete power spectrum or the structure function. The observed power spectrum and structure function can both suffer from windowing effects caused by the finite duration and sampling of the light curve, whereby power from high frequencies can leak to low frequencies (aliasing), and power at low frequencies can leak to high frequencies (e.g., red noise leak). For ground-based optical observations, an additional complication is the periodicity enforced in the sampling caused by the Earth's rotation around the sun, as objects are only observable during certain times of the year. For example, this periodic sampling can be seen in the light curve for the *MACHO* source shown in Figure 4. All of these effects can bias the power spectrum or structure function when estimated directly from the light curve in a nonparametric fashion. Similarly, these effects can bias parameter estimates when fitting a model to the observed power spectrum or structure function.

In contrast, estimating a "characteristic" timescale and variance directly from the observed time series, instead of from the observed power spectrum or structure function, has the advantage of being free of windowing effects, giving unbiased estimates of τ and σ^2. Of course, this requires one to assume a parametric model for the time series (or power spectrum), but as we will show below the CAR(1) process provides a good description of most of the AGN light curves analyzed in this work. Furthermore, higher order terms can be added to Equation (1) to allow additional flexibility (e.g., Brockwell & Davis 2002), but this is beyond the scope of the current work.

When the light curve is measured with error, the likelihood function can be calculated using a "state-space" representation of the time series (e.g., Brockwell & Davis 2002). Denoting the measured fluxes as $x_1, \ldots, x_n$, observed at times $t_1, \ldots, t_n$ with measurement error variances $\sigma_1^2, \ldots, \sigma_n^2$, the likelihood function, $p(x_1, \ldots, x_n | b, \sigma, \tau)$, is a product of Gaussian functions:

$$p(x_1, \ldots, x_n | b, \sigma, \tau) = \prod_{i=1}^{n} \left[2\pi\left(\Omega_i + \sigma_i^2\right)\right]^{-1/2} \times \exp\left\{-\frac{1}{2}\frac{\left(\hat{x}_i - x_i^*\right)^2}{\Omega_i + \sigma_i^2}\right\} \quad (6)$$

$$x_i^* = x_i - b\tau \quad (7)$$

$$\hat{x}_1 = 0 \quad (8)$$

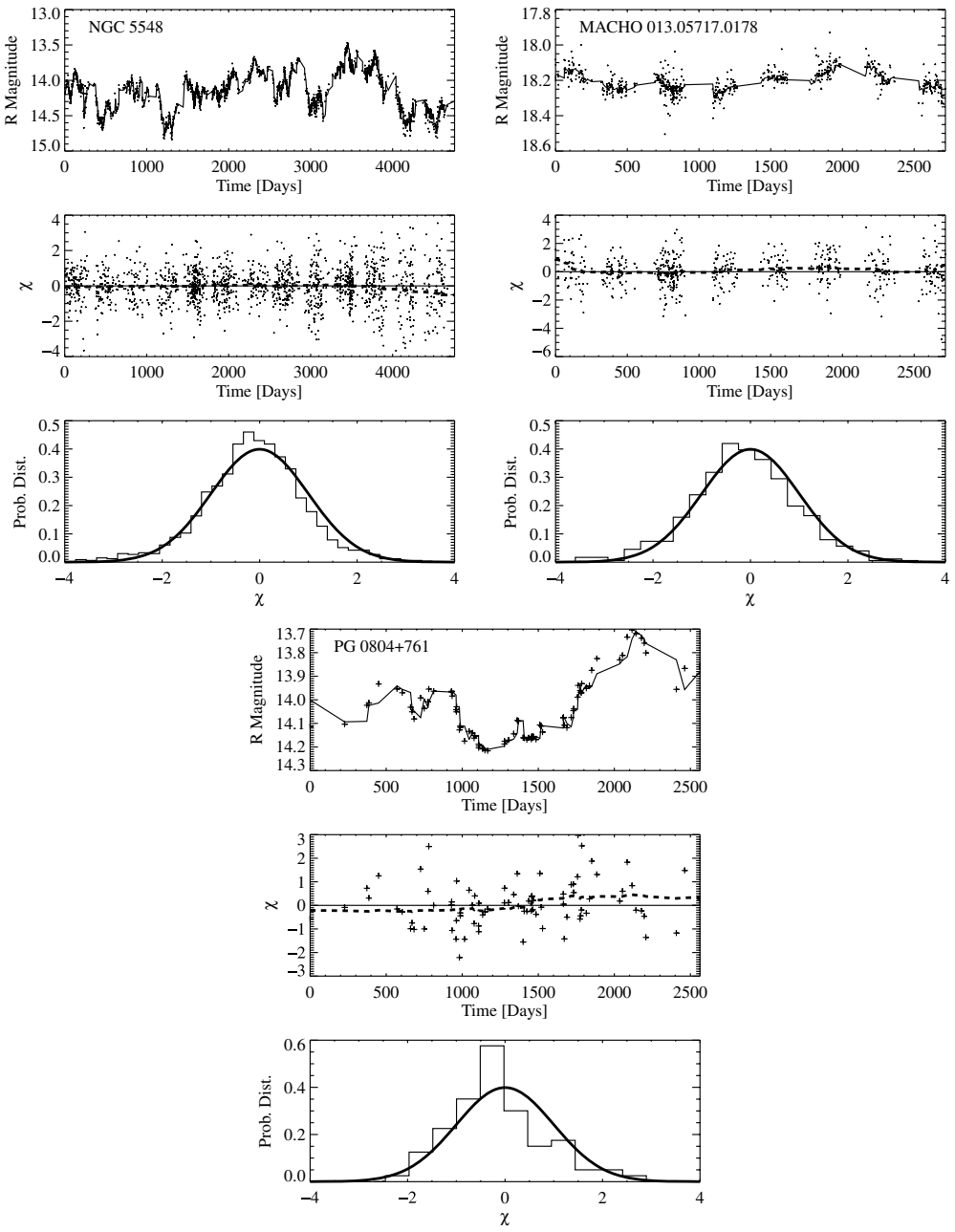

Figure 4. Light curves and best-fit CAR(1) processes for NGC 5548 (left), MACHO source 013.05717.0178 (middle), and PG 0804+761 (right). The top panels show the light curves (data points) along with the best-fit CAR(1) process (solid line), the middle panels show the standardized residuals (Equation (13)) as a function of time (data points) and a moving average estimate (dashed line), and the bottom panels compare a histogram of the standardized residuals with the expected standard normal distribution. The AGN light curves are well described by a CAR(1) process with characteristic timescales $\tau = 214$, 6026, and 1148 days for NGC 5548, MACHO 013.05717.0178, and PG 0804+761, respectively.

$$\Omega_1 = \frac{\tau\sigma^2}{2} \tag{9}$$

$$\hat{x}_i = a_i\hat{x}_{i-1} + \frac{a_i\Omega_{i-1}}{\Omega_{i-1}+\sigma_{i-1}^2}\left(x_{i-1}^* - \hat{x}_{i-1}\right) \tag{10}$$

$$\Omega_i = \Omega_1\left(1-a_i^2\right) + a_i^2\Omega_{i-1}\left(1 - \frac{\Omega_{i-1}}{\Omega_{i-1}+\sigma_{i-1}^2}\right) \tag{11}$$

$$a_i = e^{-(t_i - t_{i-1})/\tau}. \tag{12}$$

Note that Equations (8) and (9) are only valid for $i = 1$, while Equations (10)–(12) are only valid for $i > 1$. The maximum likelihood estimate is then found by maximizing Equation (6) with respect to b, τ, and σ.

In this work, we employ a Bayesian approach in order to directly compute the probability distribution of b, τ, and σ, given our observed light curves. The probability distribution of the parameters, given the observed data (i.e., the *posterior* distribution), is calculated as the product of the likelihood function with a prior probability distribution. In this work, we assume a uniform prior on b and σ. For deriving a prior on τ, we note that when the data are regularly sampled, the CAR(1) process reduces to the AR(1) process described by Equation (A1) in the Appendix with $\alpha_{\rm AR} = e^{-\Delta t/\tau}$, where Δt is

the time sampling interval. In this work, we assume a uniform prior on $\alpha_{\rm AR}$. For an AR(1) process, $\alpha_{\rm AR}$ gives the correlation between x_i and x_{i-1}. Therefore, we consider it reasonable to assume that any value of $\alpha_{\rm AR}$ is a priori likely, i.e., we do not assume anything a priori about the correlations between subsequent data points, and therefore we assume a uniform prior on $\alpha_{\rm AR}$ from 0 to 1. This prior is noninformative in the sense that all of the information on $\alpha_{\rm AR}$ comes from the data.

The accuracy of the fit can be assessed by comparing the residuals of the light curve with the values expected under the assumption of a CAR(1) process. Equation (6) implies that if the CAR(1) process provides a good model of the observed data, then the residuals should be uncorrelated and follow a normal distribution:

$$\chi \equiv \frac{x_i^* - \hat{x}_i}{\sqrt{\Omega_i + \sigma_i^2}} \sim N(0, 1). \quad (13)$$

Here, the notation $\chi \sim N(0, 1)$ means that χ is distributed according to a normal distribution with mean equal to zero and variance equal to one. The goodness of fit can then be assessed by inspecting a plot of the residuals with time to ensure that they are uncorrelated, and by comparing a histogram of the residuals with the expected standard normal distribution.

3.2. Fitting the Quasar Light Curves

In this work, we model the logarithm of the flux as following a CAR(1) process, or equivalently the apparent magnitudes. We do this because the assumption of a Gaussian white noise process in Equation (1) produces both positive and negative values of $X(t)$, while flux is a strictly positive quantity. The logarithm function maps a strictly positive quantity to the interval $(-\infty, \infty)$, and therefore Equation (1) is likely to be a better description of the light curve for the source apparent magnitude, as opposed to the source flux. Uttley et al. (2005) have also argued for describing accreting black holes as a Gaussian stochastic process in the logarithm of the flux.

An additional correction is needed to correct for cosmological time dilation. Because the quasars are fit in the observed frame, and timescales decrease as $(1 + z)$, spurious correlations may arise if one does not correct to the quasar rest frame. This is particularly problematic when dealing with flux-limited samples, which create an artificial correlation between z and both luminosity and $M_{\rm BH}$. Noting that $dt_{\rm obs} = (1 + z)dt_{\rm rest}$, Equation (1) can be expressed in the forms

$$dX(t) = -\frac{1}{\tau_{\rm obs}} X(t) dt_{\rm obs} + \sigma_{\rm obs}\sqrt{dt_{\rm obs}}\epsilon(t) + b_{\rm obs}\, dt_{\rm obs} \quad (14)$$

$$= -\frac{1+z}{\tau_{\rm obs}} X(t) dt_{\rm rest} + \sigma_{\rm obs}\sqrt{(1+z)dt_{\rm rest}}\epsilon(t) + (1+z) b_{\rm obs}\, dt_{\rm rest} \quad (15)$$

$$= -\frac{1}{\tau_{\rm rest}} X(t) dt_{\rm rest} + \sigma_{\rm rest}\sqrt{dt_{\rm rest}}\epsilon(t) + b_{\rm rest}\, dt_{\rm rest}. \quad (16)$$

From Equations (14)–(16), it is apparent that the observed and rest-frame parameters are related as

$$\tau_{\rm rest} = (1 + z)^{-1}\tau_{\rm obs} \quad (17)$$

$$\sigma_{\rm rest} = (1 + z)^{1/2}\sigma_{\rm obs} \quad (18)$$

$$b_{\rm rest} = (1 + z) b_{\rm obs}. \quad (19)$$

Noting that the mean of the CAR(1) process is $b\tau$, and that the variance is $\tau\sigma^2/2$, Equations (17)–(19) imply that the mean and variance of a CAR(1) process are unaffected by cosmological time dilation. However, the variance observed from a light curve with a finite duration and sampling is still affected by time dilation, as the observed variance over a time interval Δt is the integral of Equation (2) over that time interval. In what follows, the quantities τ, σ, and b will always refer to the quasar rest-frame quantities, unless specified otherwise.

Random draws of b, τ, and σ from the posterior probability distribution are obtained using a Metropolis–Hastings algorithm. We calculated an estimate of each parameter as the median of the posterior, and the posterior medians, standard deviations, and confidence intervals are computed using these random draws. In general, the posterior median values were not significantly different from a maximum likelihood fit. The goodness of fit for the light curves was determined by examining a histogram of the residuals and a plot of the residuals against time, as described in Section 3.1. Occasionally outlying values of the flux are present for the light curves with more data points, possibly due to unidentified systematic error. These outlying data points were removed and the light curves were refit. In Figure 4, we show the light curve and best-fit CAR(1) model for the most densely sampled object in our sample, NGC 5548, for a representative light curve from the *MACHO* sample, and for a representative light curve from the PG sample of Giveon et al. (1999). In general, the CAR(1) model provided a good fit to the quasar light curves analyzed in this work, and we only flagged nine out of 109 light curves as having a bad fit. The best-fit CAR(1) parameters, along with their uncertainties, for the 100 AGNs in our sample are listed in Table 2. The nine objects for which the fit was deemed unacceptable are not used in the regression analysis.

4. RESULTS

The distribution of σ, τ, and light curve standard deviations for our sample are shown in Figure 5. The light curve standard deviation is calculated as the square root of the light curve variance, $s = \sigma\sqrt{\tau/2}$. The best-fit quasar relaxation times have a median value of 540 days and a dispersion of 0.64 dex, and show typical long-timescale optical variations of 3%–30%. However, the uncertainties on τ are large and make a considerable contribution to the observed scatter. Correcting for the contribution from the uncertainties implies an intrinsic dispersion in relaxation times of ∼0.3 dex.

In order to look for correlations of quasar variability properties on luminosity, redshift, black hole mass, and Eddington ratio, we used the linear regression method of Kelly (2007). The method of Kelly (2007) takes a Bayesian approach to linear regression, and accurately accounts for intrinsic scatter in the regression relationships, as well as measurement errors in both the dependent and independent variables. Measurement errors can be large for both the estimates of τ and $M_{\rm BH}$, and thus can have a significant effect on the observed correlations (e.g., Kelly & Bechtold 2007). Therefore, it is necessary to correct for the measurement errors when attempting to recover any underlying trends.

Table 2
Results from CAR(1) Process Fits to Quasar Light Curves

R.A. (J2000)	Decl. (J2000)	$\log \tau$[a] (day)	Conf. Int. for $\log \tau$ (95%, day)	$\log \sigma$[b] (mag day$^{-1/2}$)	Err. in $\log \sigma$
00 29 13.7	+13 16 03.9	3.44	[2.59,6.17]	−1.97	0.05
00 47 15.8	−72 41 12.2	... [c]	...	...	...
00 49 34.4	−72 13 09.0	2.97	[2.33,5.50]	−1.95	0.05
00 51 16.9	−72 16 51.1	2.10	[1.84,2.70]	−1.60	0.03
00 54 52.1	+25 25 39.0	2.71	[2.18,4.82]	−1.81	0.05
00 55 34.2	−72 28 30.0	2.56	[2.08,4.14]	−2.31	0.06
00 55 59.6	−72 52 45.1	3.07	[2.38,6.86]	−1.85	0.02
01 01 27.8	−72 46 14.4	3.04	[2.39,5.22]	−2.04	0.04
01 02 14.4	−73 16 26.8	2.75	[2.22,5.28]	−2.23	0.05
01 02 34.7	−72 54 22.2	2.41	[2.04,3.96]	−1.80	0.03
01 07 21.7	−72 48 45.8	2.34	[2.00,3.74]	−1.89	0.03
04 46 11.0	−72 05 09.0	3.03	[2.41,5.34]	−2.20	0.05
04 53 56.6	−69 40 36.0	1.78	[1.60,2.07]	−1.93	0.02
04 56 14.2	−67 39 10.8	3.26	[2.55,5.53]	−2.17	0.06
05 00 17.6	−69 32 16.3	... [c]	...	...	...

Notes.
[a] The logarithm of the characteristic timescale of the quasar light curve, in days.
[b] The logarithm of the standard deviation in the input process to Equation (1). The standard deviation of quasar flux variations on timescales of 1 day is expected to be equal to σ.
[c] The CAR(1) process provided a poor fit to these light curves, and the data were not used in our regression analysis.
(This table is available in its entirety in a machine-readable form in the online journal. A portion is shown here for guidance regarding its form and content.)

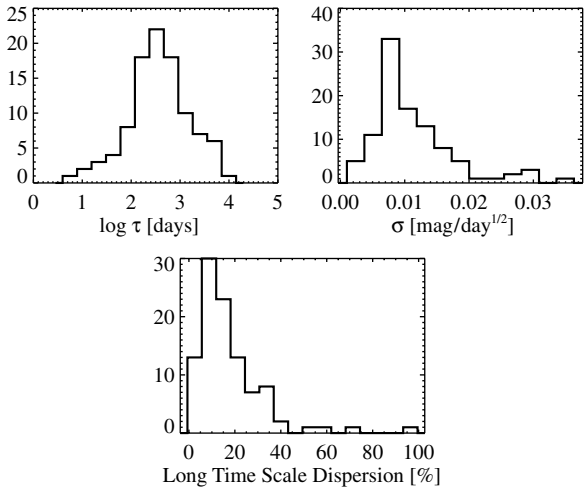

Figure 5. Distribution of the best-fit CAR(1) process parameters for the 100 quasars in our sample. The characteristic timescales of AGN optical light curves are $10 \lesssim \tau \lesssim 10^4$ days, the amplitudes of short-timescale variations are $\sigma \lesssim 0.02$ mag day$^{-1/2}$, and the amplitudes of long-timescale variations are $\lesssim$40%. The uncertainties on the characteristic timescales are large, and the true dispersion in τ is likely ∼0.3 dex.

4.1. Dependence of Quasar Variability on Luminosity and Redshift

In order to investigate whether quasar variability properties depend on luminosity, redshift, or both, we performed a regression analysis. Throughout this section, the luminosity will always be taken to be λL_λ at 5100 Å. There has been considerable debate over whether quasar variability is correlated with luminosity or redshift, and the artificial correlation between the two has made it difficult for previous work to uncover the true intrinsic correlation. However, because we perform a linear regression of variability properties on both L and z simultaneously, we are able to break the degeneracy between L and z. This is because the multiple linear regression describes how variability depends on L at a given z, and likewise for z at a given L.

In Figure 6 we show the relaxation time τ as a function of luminosity and redshift, and in Figure 7 we show σ as a function of luminosity and redshift. The results of the regressions for τ are

$$\log \tau = (-10.29 \pm 3.76) + (0.29 \pm 0.08) \log \lambda L_\lambda \ \ [\text{days}] \quad (20)$$

$$\log \tau = (2.32 \pm 0.10) + (1.12 \pm 0.41) \log(1+z) \ \ [\text{days}] \quad (21)$$

$$\log \tau = (-8.13 \pm 0.12) + (0.24 \pm 0.12) \log \lambda L_\lambda + (0.34 \pm 0.58) \log(1+z) \ \ [\text{days}], \quad (22)$$

and the results of the regression for σ are

$$\log \sigma^2 = (4.73 \pm 2.34) - (0.19 \pm 0.05) \times \log \lambda L_\lambda \ \ [R \ \text{mag}^2 \text{day}^{-1}] \quad (23)$$

$$\log \sigma^2 = (-3.84 \pm 0.06) - (0.32 \pm 0.25) \times \log(1+z) \ \ [R \ \text{mag}^2 \text{day}^{-1}] \quad (24)$$

$$\log \sigma^2 = (8.00 \pm 3.29) - (0.27 \pm 0.07) \log \lambda L_\lambda + (0.47 \pm 0.33) \log(1+z) \ \ [R \ \text{mag}^2 \text{day}^{-1}]. \quad (25)$$

There is a statistically significant correlation between τ and both L and z, where the light curve relaxation time increases with increasing L and z. In addition, there is a statistically significant anticorrelation between σ and L, implying that the short-timescale variance decreases with increasing L. However,

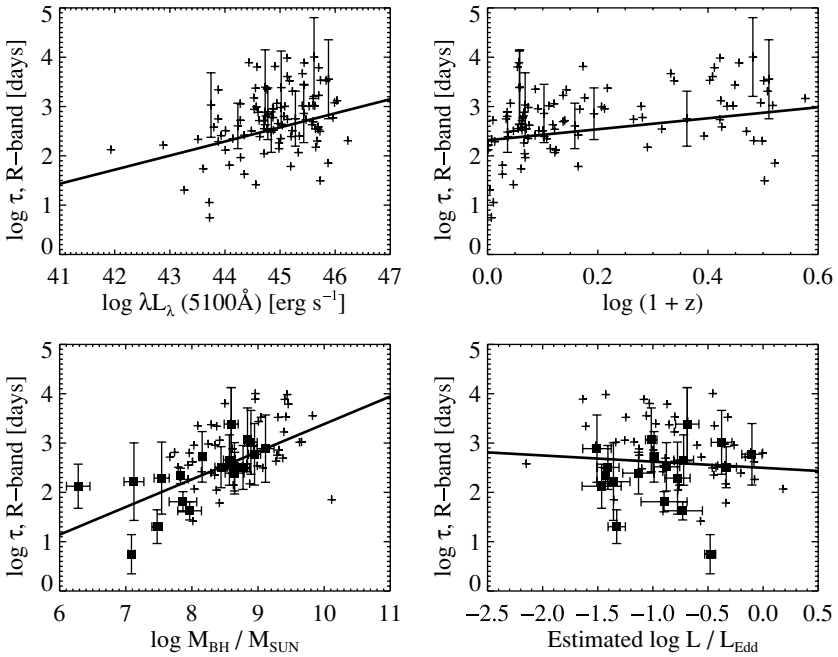

Figure 6. Characteristic timescale of the optical light curves for the AGN in our sample as a function of optical luminosity, redshift, black hole mass, and estimated Eddington ratio. For clarity, we only show error bars for a random fraction of the data points in the top two panels, and we only show the error bars for the sources with $M_{\rm BH}$ estimated from reverberation mapping in the bottom two panels. The straight lines denote the best-fit linear regression. There is a significant trend for τ to increase with increasing $M_{\rm BH}$, and less significant trends between τ and λL_λ or z. There is no significant trend between τ and $L/L_{\rm Edd}$.

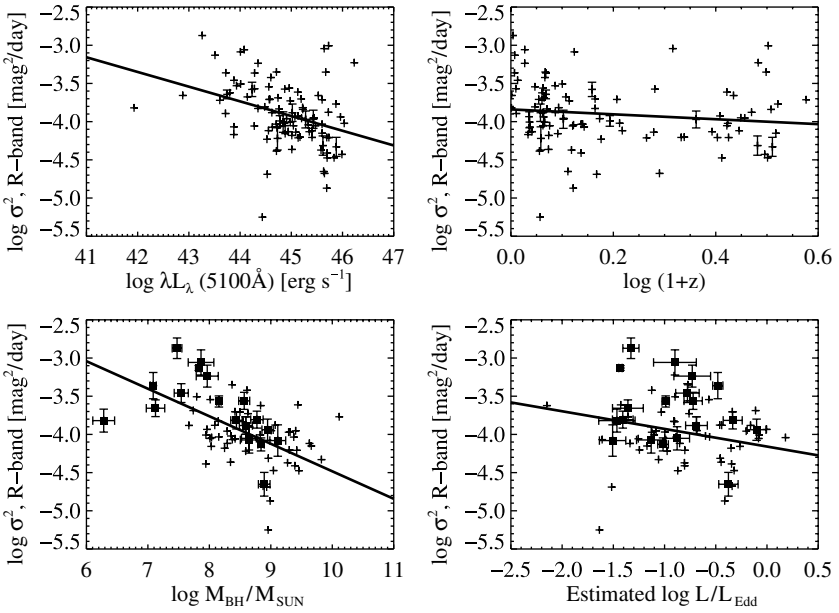

Figure 7. Same as Figure 6, but for the variance in the short-timescale variations, σ^2. There is a significant trend for σ to decrease with increasing $M_{\rm BH}$, and a similar but less significant trend between σ and λL_λ.

the multiple regression results show that the luminosity trends are the dominant ones, and that there is no significant trend between either τ or σ and z, at a given L. This therefore implies that the observed trends with redshift are caused by the artificial correlation between L and z resulting from selection effects.

We also looked for trends of the light curve variance, $\tau\sigma^2/2$, with L and z and found statistically significant evidence for a correlation between the variance of the light curve and z. Both the Spearman and Kendall rank correlation statistic was significant at 3σ, although there is considerable scatter in the correlation. This correlation is most likely a reflection of the well known fact that quasar emission at shorter wavelengths is more variable (e.g., Vanden Berk et al. 2004)

4.2. Dependence of Quasar Characteristic Timescale and Variability on M_{BH}

We also looked for trends in quasar variability properties with $M_{\rm BH}$ and the Eddington ratio, $L/L_{\rm Edd}$. In this work, we assume a constant bolometric correction of $C_{\rm bol} = 10$ to the luminosity at 5100 Å (Kaspi et al. 2000). However, we stress that a constant bolometric correction can introduce significant error

in the Eddington ratio (e.g., Vasudevan & Fabian 2007; Kelly et al. 2008), and that our use of $C_{\rm bol} = 10$ is only suggestive. Strictly speaking, what is being used in the following regressions is the ratio $\lambda L_\lambda(5100\ \text{Å})/M_{\rm BH}$, and in general this will not equal the true Eddington ratio. In Figure 6 we also show τ as a function of $M_{\rm BH}$ and $L/L_{\rm Edd}$, and in Figure 7 we also show σ as a function of $M_{\rm BH}$ and $L/L_{\rm Edd}$.

The results of the regressions for τ are

$$\log \tau = (-2.29 \pm 1.17) + (0.56 \pm 0.14) \log M_{\rm BH} \ \ [\text{days}] \quad (26)$$

$$\log \tau = (2.50 \pm 0.24) - (0.06 \pm 0.27) \log L/L_{\rm bol} \ \ [\text{days}], \quad (27)$$

and the results of the regression for σ are

$$\log \sigma^2 = (0.33 \pm 0.73) - (0.52 \pm 0.08) \times \log M_{\rm BH} \ \ [R\ \text{mag}^2\text{day}^{-1}] \quad (28)$$

$$\log \sigma^2 = (-4.33 \pm 0.19) - (0.25 \pm 0.22) \times \log L/L_{\rm Edd} \ \ [R\ \text{mag}^2\text{day}^{-1}]. \quad (29)$$

Based on these regression results, there is a statistically significant correlation between τ and $M_{\rm BH}$, where the relaxation time increases with increasing $M_{\rm BH}$. In addition, there is significant evidence that σ decreases with increasing $M_{\rm BH}$. However, there is no evidence for a dependence of τ or σ on the Eddington ratio.

In this work, we have employed the linear regression technique described in Kelly & Bechtold (2007). However, this technique assumes symmetric errors in τ, but in reality the error distribution is asymmetric. In order to assess whether this has any effects on our results, we modified the technique of Kelly & Bechtold (2007) to handle asymmetric errors in τ, and used our modified code to recompute the dependencies involving τ. However, we did not notice any difference in the slopes by assuming symmetric or asymmetric error bars. This is most likely because of the assumption of a linear relationship between $\log \tau$ and the other quantities. The asymmetric error bars for the high-mass quasars imply that the variability timescales for these sources are consistent with timescales much longer than the span of the light curve, which would lead to a steepening in the slope. However, this steepening of the slope would be inconsistent with the (better determined) timescales for the low-mass AGN, since a steeper line would predict shorter timescales than are observed. So, the assumption of a linear relationship, in combination with the well determined timescales at the low-mass end, counteracts the effects of the asymmetric error bars at the high-mass end. However, if we were to assume a nonlinear form for the dependence of $\log \tau$ on $\log M_{\rm BH}$, such that the slope increases for the high-mass objects, then the asymmetric error bars would likely have a noticeable effect, since the low-mass objects would no longer convey a lot of "information" about the regression relationship at the high-mass end.

Due to the correlation between L and $M_{\rm BH}$, it is unclear whether the observed dependency of τ and σ on these quantities is real for both L and $M_{\rm BH}$, or whether one correlation is simply a reflection of the other. Similar to breaking the L–z degeneracy, we can investigate which correlation is the fundamental one, or if both are, by performing a multiple regression of τ and σ on L and $M_{\rm BH}$. The results are

$$\log \sigma^2 = (-3.83 \pm 0.17) - (0.09 \pm 0.19) \log \left(\frac{\lambda L_\lambda}{10^{45}\ \text{erg s}^{-1}} \right) - (0.25 \pm 0.24) \log \left(\frac{M_{\rm BH}}{10^8\ M_\odot} \right) \ \ [R\ \text{mag}^2\text{day}^{-1}] \quad (30)$$

$$\tau = (80.4^{+66.9}_{-35.8}) \left(\frac{\lambda L_\lambda}{10^{45}\ \text{erg s}^{-1}} \right)^{-0.42 \pm 0.28} \times \left(\frac{M_{\rm BH}}{10^8\ M_\odot} \right)^{1.03 \pm 0.38} \ \ [\text{days}]. \quad (31)$$

Here, we have expressed τ as a function of L and $M_{\rm BH}$ instead of $\log \tau$ for more direct comparison with the characteristic timescales described by Equations (3)–(5). The joint probability distributions of the slopes are shown in Figure 8 for both regressions. It is unclear whether σ depends on solely $M_{\rm BH}$, solely L, or both $M_{\rm BH}$ and L, although the data favor a dependence on $M_{\rm BH}$ over one on L. However, there is significant evidence that the relaxation timescale depends on at least $M_{\rm BH}$, and possibly on L as well. In fact, the dependence of τ on $M_{\rm BH}$ has steepened, and the relationship described by Equation (31) is similar to that for the orbital or thermal timescale. Recent observations of quasar microlensing variability imply a size of the R-band emitting region of $R_S \sim 100$ (Morgan et al. 2007). This, in combination with our results, implies a viscosity parameter of $\alpha \sim 10^{-3}$.

5. DISCUSSION

5.1. Comparison with Previous Work

Most previous work on quasar optical variability has been based on analysis of structure functions or power spectra, either of individual quasars or an ensemble of quasars. From these studies, an anticorrelation between variability and luminosity has often emerged (e.g., Hook et al. 1994; Garcia et al. 1999; Vanden Berk et al. 2004; Wilhite et al. 2008), while results on a variability–redshift correlation have remained mixed. Our result that long-term quasar variability is uncorrelated with luminosity may appear to be in conflict with previous work. However, the evidence for a variability–luminosity correlation is considerably weaker in the studies that have computed variability measures for individual objects. Indeed, studies that have compared variability with luminosity for individual objects have noted the significant scatter in the relationship, producing a very weak correlation, often leading to a detection of "moderate" statistical significance at best. Ensemble studies, on the other hand, cannot investigate the scatter in the relationship and therefore cannot assess the strength of the correlation. Instead, ensemble studies simply look for an average trend in variability properties, and, given enough quasars, are able to detect even a weak trend of variability with luminosity. Furthermore, quasars exhibit a range in characteristic timescale and variability amplitude at a given luminosity or black hole mass, and it is unclear how this affects an ensemble structure function or power spectrum.

Recently, Wold et al. (2007) have reported a correlation between optical variability and $M_{\rm BH}$ on timescales $t > 100$ days, but no correlation is seen on shorter timescales. In contrast, we observed an anticorrelation between $M_{\rm BH}$ and short-timescale variability, but no correlation between $M_{\rm BH}$ and long-timescale variability. The Wold et al. (2007) result is unexpected, since $M_{\rm BH}$ and L are correlated (e.g., Peterson et al. 2004), and previous studies have found that variability is anticorrelated with L, even on long timescales. The Wold et al. (2007) result is based on an ensemble structure function, and the uncertainties on the structure function for the high $M_{\rm BH}$ bins are large. Furthermore, the time sampling of the Wold et al. (2007) sample for the high $M_{\rm BH}$ bins is worse than for the low $M_{\rm BH}$ bins, and windowing effects due to the finite length of the

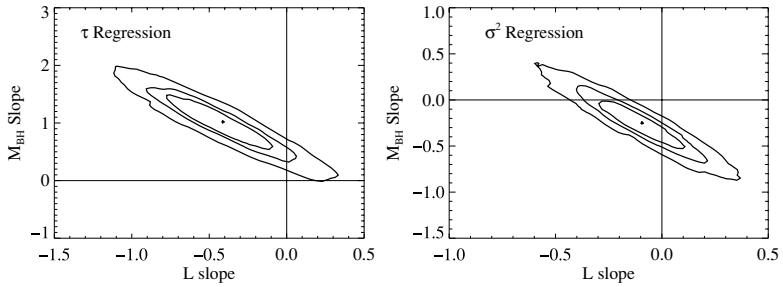

Figure 8. Posterior probability distribution for the values of the coefficients in a linear regression of the characteristic timescale of quasar optical variations, τ (left), and the magnitude of short-timescale variations, σ (right), as a function of $M_{\rm BH}$ and λL_λ (see Equations (30) and (31)). The contours correspond to approximate 50%, 75%, and 95% joint confidence regions. While there is significant evidence that τ depends on at least $M_{\rm BH}$, it is unclear if there is an additional dependence on luminosity. In addition, while it is clear that σ depends on either $M_{\rm BH}$ or λL_λ, it is unclear whether the dependency is on $M_{\rm BH}$, λL_λ, or both.

time series may be at work here. When considering variability measurement of individual sources, Wold et al. (2007) still find a positive correlation between variability and $M_{\rm BH}$. However, while this correlation is statistically significant, it is very weak and exhibits considerable scatter. We performed a Kendall and Spearman rank correlation test between long-timescale variability and the estimated black hole mass, and also find a marginally significant correlation, but the significance disappeared when we accounted for the uncertainty in the mass estimates. In addition, because the long-timescale variability for a CAR(1) process is $\tau\sigma^2/2$, Equations (26) and (28) imply that the long-timescale variability depends only weakly on $M_{\rm BH}$, if at all.

Collier & Peterson (2001) calculated structure functions of optical light curves for 12 low-z AGNs with reverberation mapping data. Consistent with our work, they find a correlation between $M_{\rm BH}$ and characteristic timescale, where a characteristic timescale was defined as the location of a break in the structure function. The timescales found by Collier & Peterson (2001) were consistent with dynamical or disk thermal timescales, although they tended to be somewhat shorter than those derived in this work. This difference may be explained by somewhat different definitions of "characteristic" timescale between their work and ours, and systematic errors in the estimated structure functions caused by time sampling effects.

Two of the sources in our sample, NGC 5548 and NGC 4151, were studied by Czerny et al. (1999, 2003), respectively, using spectral techniques. These authors fit a functional form to the optical power spectra similar to that implied by the CAR(1) model, with the exception that they allow the high-frequency slope to vary. In contrast, the CAR(1) model we employ fixes this slope to be -2, i.e., $P_X(f) \propto 1/f^2$. For NGC 5548, Czerny et al. (1999) find evidence for a flattening of the optical power spectrum on timescales $\log\tau = 3.2 \pm 0.3$ days. This is longer than our observed characteristic timescale of $\log\tau = 2.3 \pm 0.16$ at $\approx 2.5\sigma$ significance. This difference is only marginally significant, and may be explained by the slightly different parametric forms assumed for the power spectra, the longer light curve used by Czerny et al. (1999), the different photometric bands, and errors introduced by the window function and smoothing of the power spectra in the Czerny et al. (1999) analysis.

For NGC 4151, Czerny et al. (2003) did not find any evidence for a flattening to white noise of the B-band optical power spectra over the timescales probed by their 90 yr light curve. However, they find some evidence that the power spectra flattens below timescales of $\tau \sim 100$ days, in agreement with the characteristic timescale we find of $\log\tau = 2.2 \pm 0.78$ days. Furthermore, we note that our analysis constrains the characteristic timescale for NGC 4151 to be $\lesssim$30 yr at 99% confidence. If the power spectra does flatten on timescales $\sim$30 yr, it would be difficult to detect in the spectral analysis employed by Czerny et al. (2003), as such a turnover would occur in the few lowest frequency bins. This is especially true when one considers that the lowest frequency bins of the power spectra are also among the bins most biased by windowing effects and smoothing.

5.2. Connection with Accretion Physics

In this work, we have found that both the characteristic timescale of quasar light curves, and the magnitude of the short-timescale variations, depend on black hole mass. This, in combination with the evidence from reverberation mapping, strongly argues that the source of quasar optical variability is intrinsic to the accretion disk. In addition, we have found that the characteristic timescales of quasar light curves are similar to what would be expected for disk dynamical or thermal timescales, assuming a viscosity parameter of $\alpha \sim 10^{-3}$. Recent MHD simulations of radiation-dominated AGN accretion disks have found that the thermal timescale is shorter than that implied by the standard α prescription (Turner 2004), making the association of τ with thermal timescales more consistent. Our results imply that on timescales shorter than $t_{\rm orb}$ or $t_{\rm th}$, the accretion disk has difficulty generating variations in optical flux in response to random variations of some input process, such as, for example, a time-varying magnetic field. Instead, these short-timescale variations get "smoothed out," creating a $1/f^2$ power spectrum for frequencies higher than $\sim 1/t_{\rm orb}$ or $\sim 1/t_{\rm th}$.

While the quasar characteristic timescales are consistent with both orbital and thermal timescales, we find it more appropriate to associate these timescales with $t_{\rm th}$, as we might expect some sort of periodic activity in the light curves if the flux variations were driven by orbital motion. In addition, quasar optical emission is thought to be thermal emission from an optically thick accretion disk (e.g., Krolik 1999; Frank et al. 2002), and quasars tend to be bluer as they brighten (e.g., Giveon et al. 1999; Trèvese et al. 2001), suggesting that the flux variations are due to thermal variations. An association with orbital timescales cannot be ruled out, and indeed, the characteristic timescale of the turbulence driving the magnetic energy and kinetic energy density in the disk is $\sim t_{\rm orb}$ (e.g., Hirose et al. 2008). However, if the radiation energy density in the disk is due to dissipation of magnetic and kinetic energy densities, then it is expected to respond to fluctuations in the magnetic and kinetic energy densities with a characteristic timescale of the order of thermal time.

In order to interpret the CAR(1) process in terms of accretion disk physics, we rewrite Equation (1) as

$$d\log L(t) = -\frac{1}{\tau}(\log L(t) - \mu)dt + \sigma[B(t+dt) - B(t)]. \quad (32)$$

Here, $L(t)$ denotes the luminosity of the quasar at time t, $\mu = \tau b$ is the mean value of the quasar light curve, and $B(t)$ denotes Brownian motion. In Equation (32), we have used the fact that the derivative of Brownian motion is white noise, i.e., $\epsilon(t) = dB(t) = B(t + dt) - B(t)$. Brownian motion is a nonstationary random walk process that has a power spectrum $P(f) \propto 1/f^2$, and is described by Equation (1) in the limit $\tau \to \infty$. In addition, Equation (32) implicitly assumes that the variance in the random variable $dB(t) = B(t + dt) - B(t)$ is $\mathrm{Var}(dB(t)) = dt$. The notation $B(t)$ should not be confused with the common physics notation of denoting the amplitude of a magnetic field; although in this work we suggest that $B(t)$ may be associated with a turbulent magnetic field, the term $B(t)$ should be understood as referring to a Brownian motion.

Writing the equation for a CAR(1) process as Equation (32) reveals a number of interesting properties of this process. First, we note that the first term on the right side is what keeps the time series stationary. Considering only this term (i.e., $\sigma = 0$), $d \log L(t)/dt$ is negative when the value of $L(t)$ is brighter than the mean, and $d \log L(t)/dt$ is positive when $L(t)$ is fainter than the mean. Therefore, the first term on the right side stabilizes the process by always driving $L(t)$ toward its mean value, while the second term generates random perturbations to $d \log L(t)/dt$ that cause $L(t)$ to deviate from its expected path. For highly accreting objects such as quasars, the accretion disks are expected to be radiation pressure dominated in the regions emitting the optical and UV flux. Under the standard α prescription for the viscosity, where the viscous torque is assumed to be proportional to the total pressure, a radiation-pressure-dominated disk is unstable to perturbations in the heating rate (e.g., Shakura & Syunyaev 1976; Krolik 1999). The fact that the quasar light curves in our sample are described well by a CAR(1) process with relaxation times similar to disk thermal timescales rules out instabilities in the disk that grow as $\sim t_{\rm th}$, consistent with results obtained from three-dimensional MHD simulations (e.g., Turner 2004; Hirose et al. 2008).

From Equation (32), it is apparent that the stochastic input into the differential equation, which drives the random variations in L, is itself a stochastic process. In particular, a random deviation in the input process, $B(t)$, over a time interval dt causes a random perturbation to the change in $\log L(t)$ expected over the interval dt, with σ controlling how sensitive $d \log L(t)$ is to $dB(t)$. For example, the input process could be due to variations in accretion rate, or perturbations caused by a time-varying magnetic field. Indeed, recently some authors have modeled quasar X-ray variability as being driven by variations in a magnetic field, with the magnetic field density being modeled as an AR(1) process (e.g., King et al. 2004; Mayer & Pringle 2006; Janiuk & Czerny 2007).

Hirose et al. (2008) have argued for a similar interpretation of quasar optical variability, based on three-dimensional MHD simulations. They argue that fluctuations in the magnetic field are dissipated, transferring energy from the magnetic field to heat in the plasma, creating thermal fluctuations in the accretion disk. The fluctuations in the heat content of the disk then create fluctuations in $L(t)$; however, because the disk radiation cannot react to changes in heat content on timescales less than the thermal timescale, the shorter timescale fluctuations in flux are smoothed out and damped. Short-timescale variations in radiation are correlated because the radiation energy density of the disk has not had time to completely react to the change in heat content induced by the change in magnetic energy density. However, on timescales $t \gtrsim t_{\rm th}$, the disk has had time to adjust to the heat content variations, thereby "forgetting" about the previous perturbations in heat content. The result is a red noise power spectrum on timescales $t \lesssim t_{\rm th}$, and a white noise power spectrum on timescales $t \gtrsim t_{\rm th}$.

Within this interpretation, the parameter σ describes the amplitude of variations in flux caused by variations in the magnetic energy density. Therefore, the anticorrelation between σ and $M_{\rm BH}$ may imply two things. First, it may imply that the magnitude of the stochastic input process, $B(t)$, possibly associated with a turbulent magnetic field, decreases with increasing $M_{\rm BH}$. Or, it may imply that the sensitivity of changes in radiation energy density to changes in the turbulent magnetic field depends on $M_{\rm BH}$, where fluctuations in the magnetic field create smaller fluctuations in $L(t)$ as $M_{\rm BH}$ increases. Alternatively, it could imply that both effects are at work.

5.3. *Microvariability and Implications for the Radio-loud/Radio-quiet Dichotomy*

Modeling quasar variability as a stochastic process provides an opportunity to unify both short- and long-timescale variability as the result of a single process. The source of variations in radio-quiet quasar optical luminosity over timescales of hours (so-called "microvariability" or "intranight variability") has remained a puzzle, although reprocessing of X-rays or a weak blazar component have been suggested (Czerny et al. 2008). In general, microvariability in radio-quiet quasars is not detected above the photometric uncertainty (e.g., Gupta & Joshi 2005; Carini et al. 2007); however, for those sources for which it is detected the standard deviation in the variability over the course of a night is $\sim$0.01 mag (Gopal-Krishna et al. 2003; Stalin et al. 2004, 2005; Gupta & Joshi 2005). As noted in the Appendix, for a CAR(1) process the standard deviation of short-timescale variations is $\approx \sigma \sqrt{\Delta t}$. As can be seen from Figure 5, our best-fitting CAR(1) processes for quasar light curves predict variations of $\lesssim$0.02 mag over 8 hr, consistent with what has been observed for radio-quiet quasars. Furthermore, it implies that the amplitude of microvariability should decrease with increasing black hole mass.

To further investigate whether our best-fitting CAR(1) processes are consistent with observed microvariability of radio-quiet quasars, we calculate the expected distribution of microvariability amplitude for three different values of black hole mass: $M_{\rm BH} = 10^7$, 10^8, and 10^9 $M_\odot$. We simulate light curves using the values of τ and σ calculated from Equations (26) and (28) for each value of $M_{\rm BH}$. Each simulated light curve had 40 data points, regularly sampled over the course of 5 hr; these values were chosen to be consistent with recent observations of microvariability (e.g., Stalin et al. 2005; Gupta & Joshi 2005). For simplicity we neglect observational error. Following Romero et al. (1999), we calculate the amplitude of microvariability from the difference in the maximum and minimum observed flux values, expressed as a percent:

$$\psi = \frac{100}{\overline{L(t)}} \left(L_{\rm max}(t) - L_{\rm min}(t)\right). \quad (33)$$

Here, $\overline{L(t)}$ is the average value of the light curve. The results are shown in Figure 9. As can be seen, the amplitudes of microvariability expected from our best-fit CAR(1) processes are consistent with what is observed, at least for radio-quiet quasars (e.g., Gopal-Krishna et al. 2003; Stalin et al. 2004, 2005; Gupta & Joshi 2005).

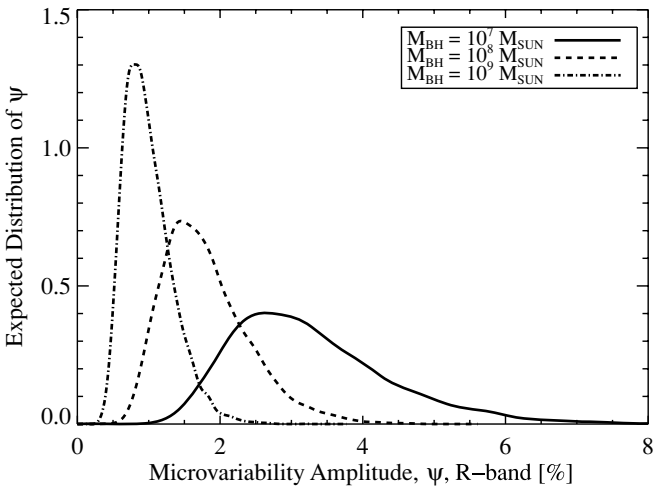

Figure 9. Expected probability distribution of radio-quiet quasar microvariability amplitude, ψ, predicted from the best-fit CAR(1) process parameters, for $M_{\rm BH} = 10^7\ M_\odot$ (solid line), $M_{\rm BH} = 10^8\ M_\odot$ (dashed line), and $M_{\rm BH} = 10^9\ M_\odot$ (dash-dotted line). The parameter ψ is defined to be the maximum observed difference in flux values observed over a 5 hr period, in percent. The amplitude of microvariability predicted from our best-fitting CAR(1) processes is consistent with what has been observed in radio-quiet quasars, implying that the same process drives both the long- and short-timescale variations in these objects.

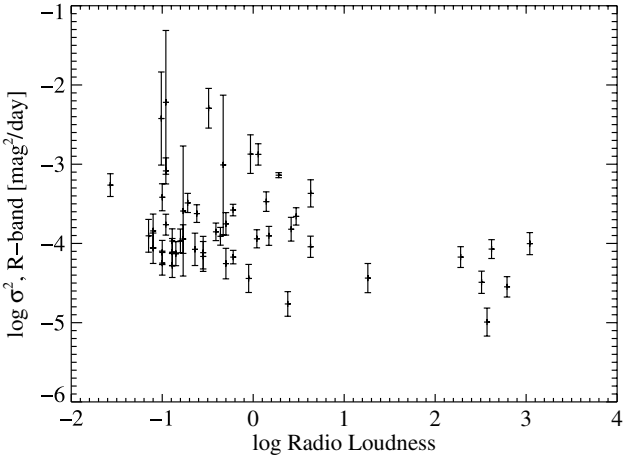

Figure 10. Best-fit values of σ as a function of radio loudness, $R_{6\,\rm cm}$. For the CAR(1) process assumed in this work, short-timescale variations have a dispersion of $\sim\sigma\sqrt{dt}$ on timescales $\approx dt$. The amplitude of microvariability decreases with increasing radio loudness, opposite the trend found from direct observations of microvariability in radio-quiet and radio-loud sources. This, along with the fact that our study only probes timescales $\gtrsim 2$ days, implies that radio-loud objects have an additional variability component that operates on intranight timescales.

Radio-loud quasars, on the other hand, are known to exhibit stronger microvariability, and the intranight fluctuations are often above the detection threshold (e.g., Gupta & Joshi 2005). If the physical mechanism for microvariability is the same in both radio-quiet quasars and radio-loud quasars, then the observational result that radio-loud quasars exhibit stronger microvariability implies a correlation between σ and radio loudness. To test this, we compare the values of the radio loudness, $R_{6\,\rm cm}$, for the Giveon et al. (1999) and AGN Watch samples. The radio-loudness parameter, $R_{6\,\rm cm}$, is defined in the standard way to be the ratio of flux density at 6 cm to the flux density at 4400 Å; the traditional division between radio-quiet and radio-loud sources occurs at $R_{6\,\rm cm} = 10$ (Kellermann et al. 1989). Figure 10 shows the best-fit values of σ^2, which give the optical variance on timescales of $\approx$1 day, as a function of radio loudness. As can be seen, σ is anticorrelated with radio loudness, showing that our best-fit CAR(1) process parameters predict microvariability should actually be reduced in radio-loud quasars. This is inconsistent with the observational result that microvariability is stronger in radio-loud quasars, and implies an additional variability mechanism in radio-loud objects on timescales shorter than those probed by our study.

Our analysis suggests that radio-loud quasars have an additional variability mechanism that operates on timescales $\lesssim$1 day. Because the time sampling for the light curves analyzed in this sample is $\gtrsim$2 days, we are only able to probe variations on timescales 2 days $\lesssim \delta t \lesssim$ 7 yr when fitting the CAR(1) process. Therefore, variations on timescales $\lesssim$1 day are not used in estimating σ. The fact that the magnitude of microvariability predicted by the best-fit CAR(1) processes for radio-quiet quasars is consistent with direct observations of microvariability implies that the microvariability in radio-quiet quasars is caused by the same process that drives the longer timescale variations. In this work, we have suggested that this process, which is well described as a CAR(1) stochastic process, is the result of a turbulent magnetic field driving thermal fluctuations in the accretion disk. If this process is also the source of microvariability in radio-loud objects, then the anticorrelation between σ and radio loudness would imply that microvariability should be reduced in radio-loud quasars. However, because the opposite is true, this implies that radio-loud objects have an additional source of variability on timescales $\lesssim$1 day, but does not operate on the timescales probed by are study, i.e., 2 days $\lesssim \delta t \lesssim$ 7 yr. This additional source of optical variability in radio-loud objects is likely due to the presence of a relativistic jet, as has often been suggested.

Because the magnitude of microvariability predicted by our best-fit CAR(1) process is consistent with observations of microvariability in radio-quiet quasars, it is not necessary to invoke an additional physical mechanism to explain the short-timescale variations in these objects. Instead, the CAR(1) process is able to explain both short- and long-timescale variations as being driven by the same process, possibly thermal fluctuations being driven by a turbulent magnetic field. Czerny et al. (2008) investigated three different models for microvariability in radio-quiet quasars and concluded that the most promising source of the microvariability was a weak blazar-like jet. Furthermore, Czerny et al. (2008) concluded that luminosity fluctuations driven by the MRI are not strong enough to create microvariability. Our empirical results are inconsistent with the conclusions of Czerny et al. (2008) in that we do not find any evidence for an additional process that drives the microvariability. This is not to say that our results imply that a weak jet does not exist in radio-quiet quasars, but rather that if a weak jet does exist then its variability amplitude is small compared to that caused by the process that also drives the longer timescale variations, such as a turbulent magnetic field.

It is unclear how sensitive the conclusions of Czerny et al. (2008) are to the specifics of their model, and the investigation of Czerny et al. (2008) does not necessarily rule a turbulent magnetic field as being the source of microvariability in radio-quiet quasars. Of particular interest is the manner in which the time dependence of the magnetic field is modeled. Czerny et al. (2008), as well as King et al. (2004), Mayer & Pringle (2006), and Janiuk & Czerny (2007), have modeled the time series of the magnetic field as an AR(1) process:

$$u_{i+1} = \alpha_{\rm AR} u_i + \epsilon_i, \tag{34}$$

where the amplitude of the local magnetic field at the ith time step is proportional to u_i, and ϵ_i is a random variable uniformly distributed between $\pm\sqrt{3}$. Because the characteristic timescale of the magnetic field development is $\tau_B \sim k_d \tau_{\rm orb}$, Czerny et al. (2008) used a time step equal to the orbital time. However, Equation (4), in combination with Figure 10 of (Czerny et al. 2008), implies that the orbital timescale should be ∼100–1000 days, depending on the mass of the black hole. This results in a time sampling of the magnetic field that is much longer than the timescales over which microvariability is measured, therefore artificially suppressing the amplitude of microvariability in the simulated light curves. Moreover, the amplitude of microvariability can also be increased by increasing the variance of the random variable ϵ_i.

Following King et al. (2004), Czerny et al. (2008) assumed a value of $\alpha_{\rm AR} = 0.5$. As described in the Appendix, a value of $\alpha_{\rm AR} = 0.5$ corresponds to a characteristic timescale for the equivalent continuous process of $\tau = 1.44\tau_{\rm orb}$, i.e., a value of $k_d = 1.44$. A more accurate simulated light curve can be obtained by using a sampling interval in Equation (34) that is small compared to that probed by microvariability, such as $\Delta t \sim$ minutes. Then, the value of α can be related to the characteristic timescale of the magnetic field development as $\alpha_{\rm AR} = \exp\{-\Delta t/(k_d\tau_{\rm orb})\}$. In this case, the only free parameters are k_d and the variance of ϵ_i. Further improvement can be obtained by employing three-dimensional MHD simulations to test whether a turbulent magnetic field can create microvariability with fluctuations ∼2%.

6. SUMMARY

In this work, we have modeled quasar light curves as a type of stochastic process called a first-order continuous autoregressive process. This statistical model has three free parameters: the characteristic timescale for the process to "forget" about itself, τ, the magnitude of the small timescale variations, σ, and the mean of the time series, μ. We used this model to fit 100 quasar light curves at $z < 2.8$, including 70 quasars with black hole mass estimates. Our conclusions are summarized as follows.

1. Quasar optical light curves are often well described by a continuous autoregressive process (CAR(1)). For the quasars in our sample, the amplitude of variations on timescales long compared to their characteristic timescales (i.e., ∼decades) are typically ∼3%–30%, consistent with previous work. The characteristic timescales of the quasar light curves vary between ∼10 days and ∼10 yr and are consistent with accretion disk orbital or thermal timescales, assuming a viscosity parameter of $\alpha \sim 10^{-3}$ and location of the emitting region to be $R_S \sim 100$. In addition, the short-timescale variations are $\lesssim$0.03 mag day$^{-1/2}$.
2. The characteristic timescales of quasar optical light curves are correlated with $M_{\rm BH}$ and luminosity, while the magnitude of the short-timescale variations are anticorrelated with $M_{\rm BH}$ and luminosity. We did not find any evidence for an additional redshift correlation. A multiple regression analysis suggested that the primary correlation is with $M_{\rm BH}$. At a given luminosity, the characteristic timescales depend on $M_{\rm BH}$ as

$$\tau = (80.4^{+66.9}_{-35.8}) \left(\frac{\lambda L_\lambda}{10^{45}\ {\rm erg\ s^{-1}}}\right)^{-0.42\pm0.28} \times \left(\frac{M_{\rm BH}}{10^8\ M_\odot}\right)^{1.03\pm0.38} \quad [{\rm days}] \qquad (35)$$

   where the errors are quoted at 68% confidence (1σ).
3. Within the CAR(1) process model of quasar light curves, the random perturbations to $d\log L(t)$ are caused by a stochastic process. This stochastic input process may be a turbulent magnetic field that creates fluctuations in the accretion disk radiation energy density. Variations in the input process over an interval dt create variations in $L(t)$ which are smoothed out on timescales shorter than an orbital or thermal timescale.
4. The fact that radio-quiet quasar optical light curves can be well fit by a CAR(1) model suggests that it is not necessary to invoke an additional physical mechanism to describe short-timescale variations in these objects. Instead, within the CAR(1) model, both short- and long-timescale variations are driven by an underlying stochastic process that causes random perturbations to $d\log L(t)/dt$. This is supported by the fact that the intranight variations predicted by our best-fit CAR(1) processes are ∼2% in the R-band, consistent with observations of intranight variability. Furthermore, our best-fit CAR(1) parameters predict an anticorrelation between radio loudness and microvariability, inconsistent with what has been observed. This suggests that radio-loud quasars have an additional optical variability mechanism that operates on timescales shorter than those probed by our study, $\lesssim$2 days.

Before concluding, we stress that the CAR(1) model is a statistical model and not a physical model. Quasar light curves are stochastic in nature (e.g., Czerny & Lehto 1997), and the dependence of luminosity on the time-varying properties of the disk is complex. In this sense, the randomness in the stochastic model is not due to that fact that the physical processes themselves are not deterministic, but rather is a reflection of our lack of knowledge of the complex physical processes that generate variations in flux. While a physical model is needed in order to interpret the stochastic model in terms of accretion disk physics, and thus lead to a proper understanding of quasar light curves, the stochastic model is sufficient for modeling the data, given our current knowledge. Furthermore, much of the mathematical formalism of accretion physics is in the language of differential equations, suggesting that stochastic differential equations are a natural choice for modeling quasar light curves.

The field of stochastic processes is a rich field with well-developed methodology, predominantly because of its importance in financial and economic modeling. We have utilized the CAR(1) model because of its simplicity, and because it allows us to perform statistical inference without having our results biased by the irregular sampling, measurement errors, and finite span of the time series. However, the CAR(1) model is the simplest of stationary continuous autoregressive processes, and additional flexibility may be achieved through the addition of higher order derivatives to Equation (1). This provides a rich and flexible method of modeling the power spectra of quasar light curves without suffering from the windowing effects that can bias traditional Fourier and structure function techniques. For example, quasi-periodic oscillations can be modeled through the addition of second-order derivatives to Equation (1), as has been done in the analysis of the frequency of sunspot numbers (Phadke & Wu 1974). In addition, Equation (1) can be generalized to a vector form, allowing the simultaneous modeling of quasar light curves across multiple observing wavelengths, and thus introducing additional constraints on physical models of quasar variability. Both the use of higher order terms and multi-wavelength modeling of quasar light curves will be the subject of future research.

A computer routine for fitting the CAR(1) model to a time series is available on request from B. Kelly.

We thank Tim Axelrod for supplying the *MACHO* light curves, and Marla Geha for providing optical spectra for a number of the *MACHO* sources and providing helpful comments on an early draft of this paper. We would also like to thank Christopher S. Kochanek for comments on this manuscript, and bringing to our attention a minor error regarding the indexing of Equations (8)–(12). We also thank the referee, Bożena Czerny, for a careful reading of the manuscript and comments that led to its improvement. B.K. acknowledges support from NASA through Hubble Fellowship grant HF-01220.01 awarded by the Space Telescope Science Institute, which is operated by the Association of Universities for Research in Astronomy, Inc., for NASA, under contract NAS 5-26555. A.S. acknowledges support from NASA contract NAS 8-39073 and grant number NNX07AQSSG 16610031.

APPENDIX

DESCRIPTION OF AUTOREGRESSIVE PROCESSES

The first-order autoregressive process (AR(1)) process is a well studied stochastic process (e.g., see Scargle 1981, and references therein), generated according to

$$x_i = \alpha_{\rm AR} x_{i-1} + \epsilon_i, \tag{A1}$$

where ϵ_i is a normally distributed random variable with zero mean and variance $\sigma^2_{\rm AR}$, and the data x_i are observed at regular time intervals. The parameters of the AR(1) model are $\alpha_{\rm AR}$ and $\sigma^2_{\rm AR}$, and $\alpha_{\rm AR}$ is usually constrained as $|\alpha_{\rm AR}| < 1$ in order to ensure stationarity; a time series is said to be stationary when its mean and covariance do not vary with time.[7] The case $\alpha_{\rm AR} = 1$ corresponds to a random walk. For quasar light curves, the n observed data points $x_1, \ldots, x_n$ correspond to the observed fluxes at times $t_1, \ldots, t_n$, for $t_i = t_1 + (i-1)\Delta t$.

The discrete AR(1) process is only defined for regularly sampled time series. However, astronomical time series are rarely regularly sampled, and often large gaps in time can exist. Furthermore, the AR(1) process is a discrete process, but the underlying physical process that gives rise to the observed flux is continuous. Because of these two considerations, we instead model the quasar light curves as a first-order continuous autoregressive (CAR(1)) process. As noted in Section 3, the CAR(1) process is described by the following stochastic differential equation (e.g., Brockwell & Davis 2002):

$$dX(t) = -\frac{1}{\tau}X(t)dt + \sigma\sqrt{dt}\epsilon(t) + b\,dt, \quad \tau, \sigma, t > 0, \tag{A2}$$

where τ is called the "relaxation time" of the process $X(t)$, and $\epsilon(t)$ is a white noise process with zero mean and variance equal to 1. Throughout this work we have assumed that the white noise process is also Gaussian. In the physics literature, Equation (A2) is often referred to as an Ornstein–Uhlenbeck (O–U) process, and plays a central role in the mathematics of Brownian motion; see Gillespie (1996) for a review of the O–U process.

[7] Technically, this is referred to as "weakly stationary," while stationarity in the strictest sense implies that the probability distribution of the time series does not change with time. However, because we are only concerned with Gaussian processes in this work, the two definitions are equivalent.

The solution to Equation (A2) is

$$X(t) = e^{-t/\tau}X(0) + b\tau(1-e^{-t/\tau}) + \sigma\int_0^t e^{-(t-s)/\tau}dB(s). \tag{A3}$$

Here, $X(0)$ is a random variable describing the initial value of the time series, $dB(s)$ is a temporally uncorrelated normally distributed random variable with zero mean and variance dt. Strictly speaking, $dB(t)$ is an interval of Brownian motion, and the integral on the right side represents the stochastic component of the time series. From Equation (A3) it can be seen that if $\sigma = 0$, i.e., if there is no stochastic component, and if $X(0)$ represents a random perturbation, $X(t)$ relaxes to its mean value with an e-folding timescale τ; hence the identification of τ as the relaxation time. If $\sigma > 0$, then the path that $X(t)$ takes will vary randomly about the expected exponential relaxation.

The expected value of $X(t)$ given $X(s)$ for $s < t$ is

$$E(X(t)|X(s)) = e^{-\Delta t/\tau}X(s) + b\tau(1 - e^{-\Delta t/\tau}) \tag{A4}$$

and the variance in $X(t)$ given $X(s)$ is

$$\mathrm{Var}(X(t)|X(s)) = \frac{\tau\sigma^2}{2}[1 - e^{-2\Delta t/\tau}], \tag{A5}$$

where $\Delta t = t - s$. If $2\Delta t/\tau \ll 1$, then Equation (A5) implies that the variance on timescales much shorter than the relaxation time is $\approx \sigma^2\Delta t$. Therefore, σ^2 can be interpreted as representing the variance in the light curve on short timescales. In addition, one can show that when the time sampling is regular with $\Delta t = 1$, then the CAR(1) process reduces to an AR(1) process with $\alpha_{\rm AR} = e^{-1/\tau}$ and $\sigma^2_{\rm AR} = \tau\sigma^2(1 - e^{-2/\tau})/2$.

In astronomical time series analysis, it is common to interpret a light curve in terms of its autocorrelation function and power spectrum. The autocovariance function at time t' is defined to be the expected value of the product of $X(t)$ and $X(t + t')$, and the autocorrelation function is calculated by dividing the autocovariance function by the variance of the time series. The autocorrelation function of the CAR(1) process is

$$ACF(t') = e^{-t'/\tau}. \tag{A6}$$

Equation (A6) states that the correlations in CAR(1) light curve fall off exponentially with lag t', with an e-folding time equal to the relaxation time, τ. Following Gillespie (1996), the power spectrum of a process is computed from the autocovariance function $r_X(t')$ as

$$P_X(f) = 4\int_0^\infty r_X(t')\cos(2\pi f t')\,dt', \quad f \geqslant 0. \tag{A7}$$

For a CAR(1) process, $r_X(t') = (\tau\sigma^2/2)e^{-t'/\tau}$, from which it follows that the power spectrum of a CAR(1) process is

$$P_X(f) = \frac{2\sigma^2\tau^2}{1 + (2\pi\tau f)^2}. \tag{A8}$$

The power spectrum of the CAR(1) process falls off as $1/f^2$ on timescales short compared to the relaxation time, and flattens to white noise at timescales long compared to the relaxation time.

REFERENCES

Alcock, C., et al. 1997, ApJ, 486, 697
Alcock, C., et al. 1999, PASP, 111, 1539

Aretxaga, I., Cid Fernandes, R., & Terlevich, R. J. 1997, MNRAS, 286, 271
Balbus, S. A., & Hawley, J. F. 1991, ApJ, 376, 214
Balbus, S. A., & Hawley, J. F. 1998, Rev. Mod. Phys., 70, 1
Brockwell, P. J., & Davis, R. A. 2002, Introduction to Time Series and Forecasting (2nd ed.; New York: Springer)
Carini, M. T., Noble, J. C., Taylor, R., & Culler, R. 2007, AJ, 133, 303
Carone, T. E., et al. 1996, ApJ, 471, 737
Cid Fernandes, R. J., Aretxaga, I., & Terlevich, R. 1996, MNRAS, 282, 1191
Cid Fernandes, R., Sodré, L., Jr., & Vieira da Silva, L., Jr. 2000, ApJ, 544, 123
Collier, S., & Peterson, B. M. 2001, ApJ, 555, 775
Collier, S. J., et al. 1998, ApJ, 500, 162
Cristiani, S., Trentini, S., La Franca, F., Aretxaga, I., Andreani, P., Vio, R., & Gemmo, A. 1996, A&A, 306, 395
Cristiani, S., Vio, R., & Andreani, P. 1990, AJ, 100, 56
Cutri, R. M., Wisniewski, W. Z., Rieke, G. H., & Lebofsky, M. J. 1985, ApJ, 296, 423
Czerny, B., Doroshenko, V. T., Nikołajuk, M., Schwarzenberg-Czerny, A., Loska, Z., & Madejski, G. 2003, MNRAS, 342, 1222
Czerny, B., & Lehto, H. J. 1997, MNRAS, 285, 365
Czerny, B., Schwarzenberg-Czerny, A., & Loska, Z. 1999, MNRAS, 303, 148
Czerny, B., Siemiginowska, A., Janiuk, A., & Gupta, A. C. 2008, MNRAS, 386, 1557
de Vries, W. H., Becker, R. H., White, R. L., & Loomis, C. 2005, AJ, 129, 615
di Clemente, A., Giallongo, E., Natali, G., Trevese, D., & Vagnetti, F. 1996, ApJ, 463, 466
Frank, J., King, A., & Raine, D. 2002, Accretion Power in Astrophysics (3rd ed.; Cambridge: Cambridge Univ. Press)
Garcia, A., Sodré, L., Jablonski, F. J., & Terlevich, R. J. 1999, MNRAS, 309, 803
Geha, M., et al. 2003, AJ, 125, 1
Gillespie, D. T. 1996, Am. J. Phys., 64, 225
Giveon, U., Maoz, D., Kaspi, S., Netzer, H., & Smith, P. S. 1999, MNRAS, 306, 637
Gopal-Krishna Stalin, C. S., Sagar, R., & Wiita, P. J. 2003, ApJ, 586, L25
Gupta, A. C., & Joshi, U. C. 2005, A&A, 440, 855
Hawkins, M. R. S. 2000, A&AS, 143, 465
Hawkins, M. R. S. 2007, A&A, 462, 581
Helfand, D. J., Stone, R. P. S., Willman, B., White, R. L., Becker, R. H., Price, T., Gregg, M. D., & McMahon, R. G. 2001, AJ, 121, 1872
Hirose, S., Krolik, J. H., & Blaes, O. 2009, ApJ, 691, 16
Hook, I. M., McMahon, R. G., Boyle, B. J., & Irwin, M. J. 1994, MNRAS, 268, 305
Janiuk, A., & Czerny, B. 2007, A&A, 466, 793
Janiuk, A., Czerny, B., & Siemiginowska, A. 2000, ApJ, 542, L33
Janiuk, A., Czerny, B., & Siemiginowska, A. 2002, ApJ, 576, 908
Kaspi, S., Smith, P. S., Netzer, H., Maoz, D., Jannuzi, B. T., & Giveon, U. 2000, ApJ, 533, 631
Kaspi, S., et al. 1996, ApJ, 470, 336
Kawaguchi, T., Mineshige, S., Umemura, M., & Turner, E. L. 1998, ApJ, 504, 671
Kellermann, K. I., Sramek, R., Schmidt, M., Shaffer, D. B., & Green, R. 1989, AJ, 98, 1195
Kelly, B. C. 2007, ApJ, 665, 1489
Kelly, B. C., & Bechtold, J. 2007, ApJS, 168, 1
Kelly, B. C., Bechtold, J., Trump, J. R., Vestergaard, M., & Siemiginowska, A. 2008, ApJS, 176, 355
King, A. R., Pringle, J. E., West, R. G., & Livio, M. 2004, MNRAS, 348, 111
Krolik, J. H. 1999, Active Galactic Nuclei: From the Central Engine to the Galactic Environment (Princeton, NJ: Princeton Univ. Press)
Lightman, A. P., & Eardley, D. M. 1974, ApJ, 187, L1
Lub, J., & de Ruiter, H. R. 1992, A&A, 256, 33
Lyubarskii, Y. E. 1997, MNRAS, 292, 679
Mayer, M., & Pringle, J. E. 2006, MNRAS, 368, 379
Merloni, A. 2003, MNRAS, 341, 1051
Merloni, A., & Fabian, A. C. 2002, MNRAS, 332, 165
Morgan, C. W., Kochanek, C. S., Morgan, N. D., & Falco, E. E. 2007, ApJL, submitted (arXiv:0707.0305)
Nayakshin, S., Rappaport, S., & Melia, F. 2000, ApJ, 535, 798
Pessah, M. E., Chan, C.-K., & Psaltis, D. 2008, MNRAS, 383, 683
Peterson, B. M., et al. 2000, ApJ, 542, 161
Peterson, B. M., et al. 2002, ApJ, 581, 197
Peterson, B. M., et al. 2004, ApJ, 613, 682
Phadke, M. S., & Wu, S. M. 1974, J. Am. Stat. Assoc., 69, 325
Richards, G. T., et al. 2001, AJ, 121, 2308
Romero, G. E., Cellone, S. A., & Combi, J. A. 1999, A&AS, 135, 477
Santos-Lleó, M., et al. 2001, A&A, 369, 57
Scargle, J. D. 1981, ApJS, 45, 1
Shakura, N. I., & Syunyaev, R. A. 1973, A&A, 24, 337
Shakura, N. I., & Syunyaev, R. A. 1976, MNRAS, 175, 613
Shemmer, O., et al. 2001, ApJ, 561, 162
Siemiginowska, A., & Czerny, B. 1989, MNRAS, 239, 289
Spergel, D. N., et al. 2003, ApJS, 148, 175
Stalin, C. S., Gopal-Krishna Sagar, R., & Wiita, P. J. 2004, MNRAS, 350, 175
Stalin, C. S., Gupta, A. C., Gopal-Krishna Wiita, P. J., & Sagar, R. 2005, MNRAS, 356, 607
Starling, R. L. C., Siemiginowska, A., Uttley, P., & Soria, R. 2004, MNRAS, 347, 67
Stella, L., & Rosner, R. 1984, ApJ, 277, 312
Stirpe, G. M., et al. 1994, ApJ, 425, 609
Svensson, R., & Zdziarski, A. A. 1994, ApJ, 436, 599
Szuszkiewicz, E. 1990, MNRAS, 244, 377
Trèvese, D., Kron, R. G., & Bunone, A. 2001, ApJ, 551, 103
Trèvese, D., & Vagnetti, F. 2002, ApJ, 564, 624
Turner, N. J. 2004, ApJ, 605, L45
Ulrich, M.-H., Maraschi, L., & Urry, C. M. 1997, ARA&A, 35, 445
Uttley, P., McHardy, I. M., & Vaughan, S. 2005, MNRAS, 359, 345
van der Klis, M. 1997, in Statistical Challenges in Modern Astronomy II ed. G. J. Babu & E. D. Feigelson (Berlin: Springer), 321
Vanden Berk, D. E., et al. 2004, ApJ, 601, 692
Vasudevan, R. V., & Fabian, A. C. 2007, MNRAS, 381, 1235
Vestergaard, M., & Osmer, P. 2009, ApJ, submitted
Vestergaard, M., & Peterson, B. M. 2006, ApJ, 641, 689
Wilhite, B. C., Brunner, R. J., Grier, C. J., Schneider, D. P., & Vanden Berk, D. E. 2008, MNRAS, 383, 1232
Wold, M., Brotherton, M. S., & Shang, Z. 2007, MNRAS, 375, 989

The Astrophysical Journal, 732:128 (2pp), 2011 May 10 doi:10.1088/0004-637X/732/2/128

ERRATUM: "ARE THE VARIATIONS IN QUASAR OPTICAL FLUX DRIVEN BY THERMAL FLUCTUATIONS?" (2009, ApJ, 698, 895)

Brandon C. Kelly[1,3], Jill Bechtold[2], and Aneta Siemiginowska[1]
[1] Harvard-Smithsonian Center for Astrophysics, 60 Garden Street, Cambridge, MA 02138, USA; bckelly@cfa.harvard.edu
[2] Department of Astronomy, University of Arizona, Tucson, AZ 85721, USA
Received 2011 March 28; published 2011 April 26

Online-only material: machine-readable tables

In the published paper of Kelly et al. (2009), the R.A. and decl. are incorrect for a large fraction of the objects as listed in Tables 1 and 2. This was due to an input error, and the listed R.A. and decl. do not match the other parameters for these objects. All other parameters match (e.g., luminosity, redshift, etc.), and therefore this error does not affect any of the analysis performed in Kelly et al. (2009). The corrected tables are shown here in Tables 1 and 2.

Table 1
Quasars Analyzed in This Work

R.A. (J2000)	Decl. (J2000)	z	$\log \lambda L_\lambda(5100\ \text{Å})$ (erg s^{-1})	$\log M_{\rm BH}/M_\odot$ ($M_\odot$)	Error in $\log M_{\rm BH}$[a]	Ref.[b]
00 29 13.7	+13 16 03.9	0.142	45.02	8.59	0.10	1
00 47 15.8	−72 41 12.2	2.770	45.60	···	···	2
00 49 34.4	−72 13 09.0	0.910	44.87	···	···	2
00 51 16.9	−72 16 51.1	0.490	44.90	···	···	2
00 54 52.1	+25 25 39.0	0.155	44.96	8.56	0.08	1
00 55 34.7	−72 28 34.2	0.560	44.77	···	···	2
00 55 59.6	−72 52 45.2	1.470	45.35	···	···	2
01 01 27.8	−72 46 14.4	1.050	44.93	···	···	2
01 02 14.4	−73 16 26.8	2.180	45.72	···	···	2
01 02 34.7	−72 54 22.2	2.130	45.98	···	···	2
01 07 21.7	−72 48 45.8	2.150	45.67	···	···	2
04 46 11.1	−72 05 09.8	0.950	45.64	8.87	0.46	2
04 53 56.6	−69 40 36.0	0.280	44.14	···	···	2
04 56 14.2	−67 39 10.8	0.260	44.01	7.79	0.48	2
05 00 17.6	−69 32 16.3	0.900	45.08	···	···	2

Notes.
[a] 1σ uncertainty on $\log M_{\rm BH}$.
[b] Reference for the optical light curve data.
References. (1) Giveon et al. 1999; (2) Geha et al. 2003; (3) Stirpe et al. 1994; (4) Peterson et al. 2000; (5) Kaspi et al. 1996; (6) Santos-Lleó et al. 2001; (7) Peterson et al. 2002; (8) Carone et al. 1996; (9) Shemmer et al. 2001; (10) Collier et al. 1998.

(This table is available in its entirety in a machine-readable form in the online journal. A portion is shown here for guidance regarding its form and content.)

[3] Hubble Fellow.

Table 2
Results from CAR(1) Process Fits to Quasar Light Curves

R.A. (J2000)	Decl. (J2000)	$\log \tau$ [a] (day)	Conf. Int. for $\log \tau$ (95%, day)	$\log \sigma$ [b] (mag day$^{1/2}$)	Error in $\log \sigma$
00 29 13.7	+13 16 03.9	3.44	[2.59,6.17]	−1.97	0.05
00 47 15.8	−72 41 12.2	3.15	[2.44,6.32]	−2.14	0.06
00 49 34.4	−72 13 09.0	2.98	[2.40,5.16]	−1.92	0.04
00 51 16.9	−72 16 51.1	3.79	[2.92,5.99]	−2.06	0.04
00 54 52.1	+25 25 39.0	2.71	[2.18,4.82]	−1.81	0.05
00 55 34.2	−72 28 30.0	3.00	[2.39,4.93]	−2.09	0.03
00 55 59.6	−72 52 45.1	2.39	[2.02,4.12]	−2.26	0.04
01 01 27.8	−72 46 14.4	... [c]	...	...	...
01 02 14.4	−73 16 26.8	1.72	[1.38,2.22]	−1.75	0.07
01 02 34.7	−72 54 22.2	3.08	[2.39,5.42]	−2.46	0.07
01 07 21.7	−72 48 45.8	2.91	[2.30,5.41]	−1.92	0.04
04 46 11.0	−72 05 09.0	2.18	[1.55,3.96]	−2.48	0.10
04 53 56.6	−69 40 36.0	2.34	[2.00,3.74]	−1.89	0.03
04 56 14.2	−67 39 10.8	2.53	[2.10,6.04]	−1.80	0.03
05 00 17.6	−69 32 16.3	3.03	[2.41,5.34]	−2.20	0.05

Notes.
[a] The logarithm of the characteristic timescale of the quasar light curve, in days.
[b] The logarithm of the standard deviation in the input process to Equation (1). The standard deviation of quasar flux variations on time scales of 1 day is expected to be equal to σ.
[c] The CAR(1) process provided a poor fit to these light curves, and the data were not used in our regression analysis.

(This table is available in its entirety in a machine-readable form in the online journal. A portion is shown here for guidance regarding its form and content.)

We thank Marion Schmitz for pointing out this error.

REFERENCES

Carone, T. E., et al. 1996, ApJ, 471, 737
Collier, S. J., et al. 1998, ApJ, 500, 162
Geha, M., et al. 2003, AJ, 125, 1
Giveon, U., Maoz, D., Kaspi, S., Netzer, H., & Smith, P. S. 1999, MNRAS, 306, 637
Kaspi, S., et al. 1996, ApJ, 470, 336
Kelly, B. C., Bechtold, J., & Siemiginowska, A. 2009, ApJ, 698, 895
Peterson, B. M., et al. 2000, ApJ, 542, 161
Peterson, B. M., et al. 2002, ApJ, 581, 197
Santos-Lleó, M., et al. 2001, A&A, 369, 57
Shemmer, O., et al. 2001, ApJ, 561, 162
Stirpe, G. M., et al. 1994, ApJ, 425, 609